ACCSCIENCE PUBLISHING

International Journal of Bioprinting

RESEARCH ARTICLE

# 3D-printed cardiac patch coated with human extracellular matrix hydrogel: Significant improvement of cell adhesion and immune reaction

**Marjan Enayati[1,2]*, Christopher Riedmüller[1,2], Sabrina Rohringer[1,2], Lukas Weber[1], Felix Pointner[1], Luis Pichelkastner[1], Marta Bonora[2,3], Ana Isabel Antunes Goncalves[1], Francesco Moscato[2,3,4], Ewald Unger[3], Emir Benca[5], Marvin Dötzlhofer[1], Bruno K. Podesser[1,2], Karl H. Schneider[1,2,4] and Helga Bergmeister[1,2]**

[1]Center for Biomedical Research and Translational Surgery, Medical University Vienna, Austria

[2]Ludwig Boltzmann Institute for Cardiovascular Research, Vienna, Austria

[3]Center for Medical Physics and Biomedical Engineering, Medical University Vienna, Austria

[4]Austrian Cluster for Tissue Regeneration, Vienna, Austria

[5]Department of Orthopedics and Trauma Surgery, Medical University Vienna, Austria

## Abstract

Constructing a cell-inductive scaffold that promotes the proliferation of cardiac-specific host cells for effective myocardium repair is a great challenge in the realm of cardiac tissue engineering. Three-dimensional (3D) printing allows for the precise fabrication of intricate structures like cardiac patches but produces large pores (sub-macron), reducing surface area for cell attachment and tissue regeneration. Moreover, the hydrophobic nature of most polyesters used in 3D printing further complicates cell adhesion and integration. In this study, human chorion placenta extracellular matrix (hpcECM) hydrogel with highly preserved ECM components, such as glycosaminoglycans (GAG), elastin, and collagen, was coated on a hydrophobic 3D-printed poly-ε-caprolactone (PCL) patch. The presence of hpcECM on the 3D-printed PCL patches could significantly induce higher levels of cell attachment, proliferation, and activation of cells such as human umbilical vein endothelial cells (HUVECs), endothelial progenitor cells (EPCs), H9c2 undifferentiated/differentiated cardiomyoblasts and fibroblasts. Fibronectin-coated samples served as controls in the experiment. Coating efficiency, hpcECM modulus of elasticity (in nanoscale), surface profile roughness, and contact angle measurements were performed and confirmed the significant potential of hpcECM as a stable, soft, hydrophilic coating matrix with low modulus of elasticity for 3D-printed synthetic constructs. Furthermore, hpcECM could modulate the high expression of inflammatory genes (CCR7 and IL-1α, expressed after 72 hours) via high expression of IL-10 in macrophages after one week. Expression of adhesion molecules (ICAM, VCAM-1, and PECAM-1) and hemolysis rate did not show statistically significant changes. All these findings highlight hpcECM as a promising immunomodulatory matrix supporting tissue-specific cell attachment and activation; particularly, hydrophobic 3D-printed constructs would outperform equivalents like fibronectin-coated constructs.

***Corresponding author:**
Marjan Enayati
(marjan.enayati@meduniwien.ac.at)

**Citation:** Enayati M, Riedmüller C, Rohringer S, et al. 3D-printed cardiac patch coated with human extracellular matrix hydrogel: Significant improvement of cell adhesion and immune reaction. *Int J Bioprint*. 2025;11(1):532-555. doi: 10.36922/ijb.6383

**Received:** November 21, 2024
**Revised:** December 23, 2024
**Accepted:** January 2, 2025
**Published Online:** January 2, 2025

**Copyright:** © 2025 Author(s). This is an Open Access article distributed under the terms of the Creative Commons Attribution License, permitting distribution, and reproduction in any medium, provided the original work is properly cited.

**Publisher's Note:** AccScience Publishing remains neutral with regard to jurisdictional claims in published maps and institutional affiliations.

***Keywords:*** 3D printing; Human placenta chorion ECM; Induced hydrophilicity; Cell adhesion; Immunomodulation

## 1. Introduction

Heart diseases such as myocardial infarction (MI) remain major causes of death and hospitalization worldwide.[1] Following MI, ventricular wall remodeling in the infarcted area reduces cardiac output and leads to scar tissue, fibrosis, or thinning.[2,3] Cardiac tissue engineering offers a promising approach for heart tissue repair. One prominent example of a product stemming from cardiac tissue engineering is a cardiac patch, which is a thin construct fixed on the patient's tissue to provide mechanical and regenerative support in order to preserve and amend the local microenvironment. The cardiac tissue engineering approach involves an accurate combination of cardiac cells and biomaterials that imitate the complexity of the native heart. Facilitating cell adhesion on biomaterials is crucial for promoting adequate cardiac cell proliferation. At present, both synthetic and natural biomaterials are used in cardiac tissue regeneration. Synthetic biomaterials, particularly aliphatic polyesters, are valued for their ease of customization, simple fabrication, good mechanical properties, and degradability.[4] However, their hydrophobic surfaces and absence of specific cell recognition sites can restrict their applications, necessitating strategies to improve cell affinity to these polymers. There are various methods appropriate to enhance the hydrophilicity and cell affinity of a hydrophobic biopolymer. These include chemical modifications (*e.g.*, introducing polar functional groups such as hydroxyl groups),[5] blending with hydrophilic counterparts like chitosan or agarose,[6] incorporation of hydrophilic additives (such as nanomaterials like hydroxyapatite [HA])[7] or surface modifications (via plasma treatment or coating).[8] Each method has its own advantages and disadvantages. Among these methods, surface coating is a straightforward method compatible with common techniques such as dip-coating or spray-coating, making it accessible for large-scale production. One ideal approach is coating with natural biomaterials and creating an extracellular matrix (ECM)-like environment that enhances early cell attachment and migration while preserving the polymer backbone's integrity.[9] Collagen, gelatin, fibrin- and ECM-based hydrogels are major natural biomaterials due to their biocompatibility, ease of handling, and natural degradability.[4,10,11] Pei et al.[12] showed that a hierarchical poly-ε–caprolactone (PCL)-HA construct could induce osteogenesis in human adipose stem cells (hASCs) in the presence of type I collagen coating and plasma surface treatment. Furthermore, gelatin-coating could enhance the adhesion of human mesenchymal stem cells and cellular bioactivity in graphene oxide-incorporated electrospun PCL constructs.[13]

However, there are still disadvantages associated with each available biomaterial in the coating approach. Collagen, derived from animals, humans, or recombinant systems, shows poor mechanical stability, immunogenicity, and rapid enzymatic degradation.[14] Gelatin, a biocompatible denatured collagen, lacks thermostability and suitable pore size, limiting its clinical use.[15] Fibronectin supports cell adhesion but may promote atherosclerotic plaque formation, warranting caution in cardiovascular applications.[16] As an example, mesenchymal stem cell-seeded fibronectin-modified PCL patches could promote neovascularization and reduce inappropriate left ventricle remodeling in an MI rat model. Despite their advantages in applications, fibronectin-immobilized PCL fibrous patch is not considered a significant stride achieved in the realm of cardiac tissue engineering.[17] Extracellular matrix from decellularized tissue (or decellularized extracellular matrix, dECM) is an optimal natural biomaterial for cell interaction, capable of mimicking native tissue environments. Nevertheless, these natural biomaterials are not without shortcomings, such as their detrimental immunogenicity against mammalian antigens (such as α-gal epitope) and their demanding production and sterilization process.[18]

In this study, the potential of a self-developed human chorion placental ECM hydrogel to increase cell adhesion and proliferation on synthetic polymer scaffolds was investigated. PCL is a polymer approved by the U.S. Food and Drug Administration (FDA), equipped with excellent biocompatibility, suitable biodegradability, and tunable mechanical properties, which are promising characteristics to withstand the challenging requirements of the cardiac environment.[19] The human placenta and its components (such as the amniotic and chorionic membrane, and the umbilical cord) are considered sources of abundant biological materials and have been applied as membranes or hydrogels in a broad range of therapies.[20] For example, decellularized placenta allograft membranes (PAM) including amnion and chorion promote faster and more organized healing in ocular tissues[21] and enable advanced wound care applications.[22] It has been reported that the application of bioengineered cardiac patches consisting of the decellularized placenta and human-induced pluripotent stem cells in an MI rodent model could significantly improve cell retention and neovascularization and reduce infarct size.[23]

Recently, there has been a strong interest in using placenta-based ECM hydrogels for the repair of ischemic myocardial tissue[24] or as a component of bioinks in 3D bioprinting technology.[25,26] However, the majority of the studies utilized the ECM of the placenta as a whole, instead of using the individual components. For example, placenta ECM bioink mixed with silk fibroin and alginate has been utilized to create scaffolds for full-thickness skin repair. The placenta ECM could enhance angiogenesis, re-epithelialization, and formation of granulation tissue in the mice wound healing model after 21 days.[27] The potential of amnion ECM as a biomaterial has been intensively investigated,[28] whereas the chorion-derived ECM is relatively unexplored. Amnion ECM hydrogels are already commercialized for wound healing applications,[29] and decellularized amnion membrane approaches have been widely used in bone regeneration applications,[30,31] where they induce an inflammatory reduction after transplantation.[32] Regarding chorion-based hydrogels, McQuilling et al.[31,33] found that native chorion membranes contain more growth factors (pg/cm$^2$) compared to amnion. However, after dehydration, the content was significantly lowered. All these findings emphasize the necessity of modifying tissue processing. Furthermore, other studies showed a higher potential of chorion in osteogenic applications[31,33] and inflammatory reduction (in the form of exosomes derived from human chorion membrane extracts)[31] compared to amnion. Our group has successfully established a method for the decellularization of chorion, a technique already applied in the creation of ECM hydrogels and small-diameter vascular grafts.[34,35].

To the best of our knowledge, there is no published literature describing the usage of human chorion placenta extracellular matrix (hpcECM) hydrogel as a component, nor as a coating agent for a 3D-printed cardiac patch. 3D printing provides precise control over the deposition of materials to form intricate structures. Nonetheless, the resolution of the pores in these constructs tends to be relatively large (with sub-macron pores), compared to other methods such as electrospinning, where sub-micron pores are created.[36] Therefore, the coating efficiency of a hydrophobic construct with large pores might be challenging, especially in the case of using less concentrated hydrogels as a coating agent. In this study, PCL patches with relatively large pores were precisely fabricated via a 3D-Bioplotter. Subsequently, patches were coated with an hpcECM hydrogel of two different concentrations (0.02% hpcECM-PCL and 0.2% hpcECM-PCL). First, the surface characteristics and efficiency of coating in terms of morphology, pore size, porosity, roughness, wettability, and mechanical properties (unidirectional tensile strain measurements and nanoindentation) were studied. Afterward, the influence of hpcECM on attachment/proliferation/activation of cardiac cells (such as endothelial progenitor cells (EPCs), endothelial cells (ECs), H9c2 differentiated/undifferentiated cardiomyoblasts, and fibroblasts), expression of adhesion molecule such as intercellular adhesion molecule 1 (ICAM-1) and vascular cell adhesion molecule 1 (VCAM-1), immunomodulatory behavior (M1 and M2 macrophages and cytokine gene expression makers), and hemocompatibility were studied. Uncoated printed PCL with and without pores and fibronectin-coated PCL patches served as controls. In this study, it was shown that the hpcECM hydrogel provided a cell-inductive environment with an excellent potential to improve the proliferation of cardiac-specific host cells as a coating interface on synthetic 3D-printed scaffolds compared to its equivalents such as fibronectin-coated constructs.

## 2. Materials and methods

### 2.1. Production and characterization of hpcECM gel

The production of hpcECM gels from the human placenta has been described previously by our group.[35] All the procedures were approved by the institutional ethics committee of Medical University of Vienna (EK-Nr.: 1602/2018), and consent was obtained from the mothers prior to tissue use. Briefly, the donated placentas were obtained from cesarean sections performed at the Department of Obstetrics and Gynecology at the Medical University of Vienna (Austria). Chorion was isolated from the basal tissue, amnion and umbilical cord. The decellularization process was conducted using 2% Triton X-100 (Sigma-Aldrich GmbH, Vienna, Austria) and 0.02% ethylenediaminetetraacetic acid (EDTA, Sigma-Aldrich GmbH, Vienna Austria) for 3 days with 3 phosphate-buffered saline (1× PBS) washing steps in between. 0.4% DNase (Roche AG, Basel, Switzerland) treatment was subsequently applied for DNA removal. Afterwards, decellularized tissues were stored in 0.18% peracetic acid in 4.8% ethanol (Sigma-Aldrich GmbH, Vienna, Austria) for 2.5 hours for sterilization. Samples were frozen at −20°C, lyophilized, and cryo-milled with a Freezer Mill 6770 (SPEX Sample Prep LLC, Metuchen, NJ, USA). Porcine gastric mucosa pepsin (Roche AG, Basel Switzerland) was used for solubilization of the chorionic powder by enzymatic digestion under acidic conditions (0.1 M HCl; Merck, Darmstadt, Germany). pH neutralization of the resulting gel using 1 M NaOH (Merck, Darmstadt, Germany) and adjusting the salt concentration to 1× were performed. The final product was stored at −80°C.

Hematoxylin and eosin (H&E) staining was conducted to validate complete cell removal from the tissue. To do so,

the tissues were paraformaldehyde-fixed, dehydrated and embedded with Tissue-Plus™ OCT Compound (Clear Cryostat Embedding Medicum; Scigen Scientific Inc., Gardena, CA, USA). Afterward, the samples were sectioned (each 20 µm) and placed on the slide for H&E staining, according to the manufacturer's protocol (Morphisto, Offenbach, Germany). To control the quality of the product, each batch of the produced hpcECM powder in the form of pre-gel solutions was examined for further biochemical quantification methods such as assessing the residual DNA, elastin, glycosaminoglycan (GAG), and collagen content. Briefly, DNA Extraction Mini Kit (Favorgen, Taipei, Taiwan) and AccuBlue® High Sensitivity dsDNA Quantitation Kit (Biotium, Fremont, CA, USA) were used for DNA extraction and quantification. Collagen content was assessed by measuring the hydroxyproline content of neutralized samples following hydrolysis in 6 M HCl at 110°C for 20 hours. 1,9-dimethyl-methylene blue (DMB; Sigma-Aldrich GmbH, Vienna, Austria) staining of the pre-gel samples was conducted to identify the sulfated GAG content. Fastin™ Elastin Assay (Biocolor, Carrickfergus, UK) was utilized to assess the elastin content.

### 2.2. 3D printing of the scaffolds and morphological studies

The EnvisionTEC 3D-Bioplotter (EnvisionTEC GmbH, Gladbeck, Germany), a 3D printing tool based on a pneumatic extrusion system was used to fabricate PCL (Mn 45000 kDa; Sigma-Aldrich, St. Louis, MO, USA) based porous thin patches. These patches were designed using Magics EnvisionTEC (V13; Materialise, Leuven, Belgium), Bioplotter RP V2.9, and VisualMachines BP V2.2 (both EnvisionTEC GmbH, Gladbeck, Germany) software. For printing, pure PCL pellets were heated up to 90°C, followed by dispersion through the nozzle with a diameter of 400 µm and with a printing pressure of 9 bar (Table 1).

Thin patches were printed in two layers. The first one was a continuous line pattern with an additional wave-pair pattern on top (Figure 1a and 1b), printed with specific printing parameters. The utilized pneumatic extrusion technique provides high reproducibility and precise control over the pore size and shape.

**Table 1. Printing parameters.**

| Parameter | Value |
|---|---|
| Printhead temperature | 90°C |
| Platform temperature | 40°C |
| Printing pressure | 9 bar |
| Nozzle diameter | 400 µm |
| Pre-flow | 0.08 s |
| Post-flow | –0.12 s |
| Wait time between layers | 120 s |

### 2.3. Structural analysis, coating visualization, roughness and surface profile

The morphology and size of the pores were investigated utilizing scanning electron microscopy (SEM) images. To investigate pore size, five samples (1 × 0.5 cm) from each group (0.02% hpcECM-PCL, 0.2% hpcECM-PCL, and uncoated PCL) were prepared. Subsequently, five random positions from each sample have been selected and analyzed using ImageJ (version 2.14.0/1.54f). For each group, the surface area of 100 pores was measured and compared. Further, the porosity of the coated and uncoated samples was calculated by a gravimetric method from the known mass and the measured dimensions of the 3D-printed patches as earlier described ($n$ = 5).[37] Immunofluorescence staining against fibronectin was performed to detect the coating layer as hpcECM contains various basal lamina proteins, fibronectin, laminin, and collagen.[35] Polymer samples were cut into 1 × 0.5 cm pieces and placed into 24-well plates. Coating with 0.02% hpcECM-gel (0.2 mg/mL), 0.2% hpcECM-gel (2 mg/mL), 0.02 % fibronectin (0.2 mg/mL), and 0.1% (1 mg/mL) was performed for 2 and 72 hours at 37°C. Previously, it was shown that the higher concentration of fibronectin (at 2 mg/mL) did not result in significant differences in terms of cell adhesion or coating efficiency (data not shown) compared to lower concentration of fibronectin (1 mg/mL). Uncoated samples were incubated in Phosphate-buffered saline (PBS). The specimens were fixed in 4% paraformaldehyde overnight at 4°C. Primary mouse anti-human fibronectin antibody (clone 3F12, 1:200 dilution in PBS/1% bovine serum albumin (BSA); Thermo Fisher Scientific, Vienna, Austria) and secondary goat anti-mouse 647 (Abcam, Cambridge, UK) were used. Fluorescence mounting medium (Agilent Technologies, Santa Clara, CA, USA) including 1 µM DAPI (Sigma-Aldrich GmbH, Vienna, Austria) was used prior to confocal microscopy (Zeiss LSM700, Anna Spiegel Image Facility, Austria).

Roughness and the surface profile of the patches were analyzed using a VR-5200 wide-area 3D optical microscanner/profilometer (Keyence, Keyence International, Mechelen, Belgium). High-resolution, single-shot 3D microscopic measurements were taken with a precision of 0.1 µm. The instrument recorded data from 800,000 points within four seconds at a working distance of 75 mm, while maintaining the same 0.1 µm resolution. The analysis followed the roughness standard outlined in ISO 25178-2:2012.

### 2.4. Mechanical characterizations

Mechanical characteristics of the coated and uncoated samples (0.02% hpcECM-PCL, 0.2% hpcECM-PCL, and uncoated PCL) were assessed in both macro and micro

scales via unidirectional tensile strain and nanoindentation measurements, respectively. To assess the bulk macro mechanical properties of the constructs, an Anton Paar MCR301 rheometer (Anton Paar GmbH, Graz, Austria) with a clamp system was utilized. Force-displacement data were recorded to determine ultimate tensile strength (UTS), strain at failure (SAF), and modulus of elasticity (E) ($n = 5$ per group). Tests were performed at a strain rate of 1 mm/min, with measurements taken up to the failure point of the material. UTS was calculated by normalizing the force measurements to the effective cross-sectional area. Herein, the mass of PCL was measured (1.2 mg/mm$^3$), and the effective cross-sectional area was calculated using sample dimensions (24 × 12 × 0.4 mm) and weight.

Nanoindentation was performed using the Nanoindenter ZHN (ZwickRoell GmbH & Co. KG, Ulm, Germany). Samples were attached to microscope slides using a thin two-sided adhesive tape to avoid bulking. The slides were then fixed using a clamp-type sample holder (ZwickRoell GmbH & Co. KG, Ulm, Germany). Sixteen positions were measured from each group (2 samples per group, 8 positions per sample). Each measuring point was positioned in a way to avoid interference with neighboring indents (a minimal distance of 30 μm between the points). The material's Poisson's ratio was assumed at 0.25. Indentation was performed using a Berkovich indenter with a 15 μm nominal radius. Before testing, the indenter was position-calibrated and the contact force was set at 17 μN. The measurement sequence, included a linear force slope of 1 mN/s until 10 mN maximum force was reached. The maximum force was held for 5 s before unloading to 0 mN for 4 s. The unloading curve was fitted by default between 97% and 39% of the maximum load. Before data analysis, an automatic zero-point correction was applied. No thermal drift correction was applied as the material was considered viscoelastic. Mechanical properties were calculated with the manufacturer's software (InspectorX V5.5.4; ZwickRoell GmbH & Co. KG, Ulm, Germany) for each measuring point. The position of the measuring points was controlled, following the experiments, and in case the indents were in sites of curved local surfaces, the corresponding measuring point data were excluded from the analysis. Reported data include the indentation hardness $H_{IT}$ (force divided by contact area under load) and the indentation modulus $E_{IT}$. Under ideal circumstances (no material pile-up or sink-in), the $E_{IT}$ is equal to the modulus of E.

### 2.5. Wettability and hydrophilicity characterization

Water contact angle (WCA) and free surface energy (FSE) measurements were investigated (PCL patches coated with 0.02% and 0.2% hpcECM vs uncoated samples and flat non-porous printed PCL samples). A goniometer equipped with a camera (KRÜSS DSA25, KRÜSS GmbH, Hamburg, Germany) and post-process software (ADVANCE, KRÜSS GmbH, Hamburg, Germany; and Angle Meter 360 application, AK APP Develop, Russian Federation) were employed for the WCA measurements. WCA measurement on the surfaces was performed using a 5 μL droplet of deionized water gently dispensed on the surface by a motorized syringe. WCA data on three porous and three non-porous patch samples were collected (5 WCA measurements/patch). FSE of the solid area was performed by employing the model of Owens–Wendt–Rabel & Kaelble (OWRK).[38] In the OWRK methods, contact angles of two liquids (2 μL droplets, deionized water, and diiodo-methane) with different polarities were acquired to calculate the FSE. Due to the rapid absorption of liquid through the patch (owing to the high porosity), a video of the drop deposition was recorded and the frame with a stable drop was used for the WCA calculation with the Angle Meter 360. Furthermore, to investigate the influence of the topography and exclusively study the repellent properties of the coating, PCL flat, non-porous samples with the same dimensions were printed, coated, and examined for WCA measurements.

### 2.6. Biocompatibility and cell proliferation assessments

Biocompatibility of the patches including the influence of the hpcECM coating on cell proliferation and cell viability were studied and compared utilizing human umbilical vein endothelial cells (HUVECs; Lonza Group AG, Basel, Switzerland) and human foreskin fibroblasts (HFFs; ATCC, Manassas, VA, USA). Pooled donor HUVECS were cultured in Endothelial Growth Medium 2 (EGM-2; Lonza, Wakesville, MD, USA) and HFFs were cultivated in Fibroblast Growth Medium 3 (FGM-3; Lonza, Wakesville, MD, USA). Both media were supplemented with 10% fetal bovine serum (FBS; Sigma-Aldrich GmbH, Vienna, Austria) and 1% penicillin/streptomycin (Gibco, OK, USA). After harvesting the cells at 80% confluency, HUVECs and HFFs (each at a density of 2 × $10^4$ cells/cm$^2$) were seeded on the 0.02% hpcECM-PCL, 0.2% hpcECM-PCL and uncoated sterile PCL patches (0.5 × 1 cm) in 24-well plates. After 24, 48, and 72 hours of cell cultivation, the viability of HUVECs and HFFs was quantified using a colorimetric methoxynitrosulfophenyl-tetrazolium carboxanilide (XTT) assay cell viability method utilizing 2,3-Bis(2-methoxy-4-nitro-5-sulfophenyl)-2H-tetrazolium-5-carboxanilide inner salt (XTT; Santa Cruz Biotechnology, Dallas, TX, USA) and a Spark® Multimode Microplate Reader (TECAN, TECAN Austria GmbH, Gröding, Austria).

Furthermore, live/dead assay was also applied to the H9c2 (undifferentiated and differentiated) and fibroblasts after 24 and 72 hours to determine the amount of

viable and dead cells via calcein AM (for live cells) and propidium iodide (PI; for dead cells) staining. To do so, $2 \times 1\ 0^5$ HFFs were cultured on 0.5 × 1 cm piece patches. Subsequently, cells were stained with 2.5 µg/mL PI (Sigma-Aldrich, Austria) and 1 µg/mL calcein AM Biotium, Fremont, CA, USA) for 30 min. After three washing steps and paraformaldehyde (Sigma-Aldrich GmbH, Vienna, Austria) fixation (overnight at 4°C), coated and uncoated patches were mounted using a fluorescence mounting medium and were imaged using an LSM700 confocal microscope (Zeiss, Munich, Germany).

### 2.7. Hemocompatibility assays

Blood clotting and hemolysis assays were performed. For the blood clotting assay, patches were coated with 0.02% or 0.2% hpcECM and weighed accordingly. Glass coverslips were used as positive controls. Freshly donated human blood from non-anti-coagulated volunteers was collected in EDTA tubes and recalcified (ethical committee approval number: EK Nr: 2321/2020, 10 mM $CaCl_2$; Sigma-Aldrich GmbH, Vienna, Austria). The coated patches were incubated for 1 hour at 37°C in the recalcified blood and then weighed again. The mass gained after the incubation was considered a sign of thrombus formation on the surface.

Furthermore, the hemolytic behavior of the coated patch was assessed. 0.02% and 0.2% hpcECM-coated and uncoated patches were incubated with diluted blood (1:5 dilution with 0.9% NaCl) for 1 hour at 37°C. Subsequently, samples were centrifuged (3000 rpm, 5 min) and absorbance of the supernatants was measured at 541 nm wavelength with a Spark® Multimode Microplate Reader (TECAN, TECAN Austria GmbH, Gröding, Austria). Blood diluted with distilled water (1:5 dilution) served as a positive control, whereas 0.9% NaCl (1:5 dilution) served as a negative control accordingly. Control groups did not include any constructs.

The hemolysis ratio was determined using the following formula:

$$\text{Hemolysis ratio}\,(\%) = \frac{\text{Abs}_S - \text{Abs}_{NC}}{\text{Abs}_{PC} - \text{Abs}_{NC}} \times 100 \qquad \text{(I)}$$

where $\text{Abs}_S$ is the absorbance of sample; $\text{Abs}_{NC}$ is the absorbance of negative control; and $\text{Abs}_{PC}$ is the absorbance of positive control.

### 2.8. Isolation and attachment of EPCs

EPCs were isolated from 45 mL of donated human blood (collected from healthy male and female volunteers; approved by the ethics committee: EK-NR.: 2321/2020) via density centrifugation using Ficoll Paque Plus (Cytiva, Marlborough, MA, USA). The peripheral blood mononuclear cell (PBMC) portion was isolated and washed with PBS followed by centrifugation steps. Cells were resuspended in EGM-2 medium. Polymer samples were cut into 0.5 × 1 cm pieces and placed into 24-well plates. Coating with 0.02%, 0.2% hpcECM, and 0.02% fibronectin was performed for 2 hours at 37°C. Uncoated samples were incubated in Dulbecco's phosphate-buffered saline (1× DPBS (−/−), Sigma-Aldrich GmbH, Vienna, Austria). Fibronectin-coated samples served as control. One million freshly isolated cells were seeded per PCL construct and incubated in EGM-2 medium for one week with medium changes every second day. The specimens were fixed in 4% paraformaldehyde and stained with primary mouse anti-human Prom-1 antibody (clone 2F8C5, 1:200 dilution in PBS/1% BSA; Thermo Fisher Scientific, Vienna, Austria) for 1 hour at room temperature subsequently. Goat anti-mouse 647 (Abcam, Cambridge, UK) was used as the secondary antibody. After three washing steps, samples were mounted with a mounting medium containing 1 µM DAPI (both Sigma-Aldrich GmbH, Vienna, Austria). Samples were analyzed utilizing a confocal microscope (Zeiss, LSM700).

### 2.9. Differentiated and undifferentiated H9c2 cardiomyoblast activation and proliferation

H9c2 undifferentiated cells (rat myocardial cell line) and differentiated cells (via retinoic acid [RA]) were cultured on the 0.02 % or 0.2% hpcECM-coated and uncoated samples ($2 \times 10^4$ cells/cm$^2$). XTT and live/dead assays were performed to identify cell proliferation and the amount of viable and dead cells as mentioned before (**Section 2.6**) after 24, 48, and 72 hours. Differentiation of the H9c2 cells was induced using RA. Briefly, H9c2 undifferentiated cells were cultured in DMEM with 4.5 g/L glucose, 10% FBS (Gibco, OK, USA), and 1% penicillin/streptomycin (Gibco, OK, USA) until reaching 60% confluence. Subsequently, a reduced serum concentration, at 1% FBS, was used, and 1 µg/mL of RA (Merck, Darmstadt, Germany) was added to the medium. The medium was refreshed every 24 hours for the next 5 days. On day 5, the cells were ready for further procedures. Additionally, the activation of H9c2 differentiated cells and the influence of hpcECM on the activation of H9c2 cells were studied via troponin T staining. To do so, differentiated cells were seeded into a plate ($8 \times 10^5$ cells/mL) for 24 hours. The cells were fixed in 4% paraformaldehyde (PFA) in PBS for 20 min followed by a 15-min incubation in 100 mM glycine. The cell permeabilization was performed using 0.1% Triton X-100 for 5 min. Unspecific binding sites were blocked with 4% BSA in PBS for 1 hour. The primary antibodies used were rabbit cardiac troponin T (1:200; ProteinTech, 15513-1-AP), and isolectin GS-IB4

from Griffonia simplicifolia, Alexa Fluor™ 488 Conjugate (1:200; Thermo Fisher, I21411). Secondary antibody was goat anti-rabbit IgG antibody (H+L), Texas Red (1:200; Abcam, TI-1000). Vectashield antifade mounting medium with DAPI (H-1200-10) was used to mount the coverslip on the glass slide. Samples were analyzed utilizing a Zeiss LSM700 confocal microscope (Carl Zeiss Microscopy GmbH, Germany, oberkochen).

### 2.10. Quantitation of adhesion molecule expression via RT-qPCR

Polymer samples were cut into 0.5 cm pieces and placed into 24-well plates. Coating with 0.02% or 0.2% hpcECM or 0.02% fibronectin was performed for 2 hours at 37°C. Uncoated samples were incubated in PBS (−/−). The coating solutions were then removed and HUVECs (P5-P7) were seeded to the constructs ($2 \times 10^5$ cells/specimen) for 72 hours. Cells were detached with Accutase (Sigma-Aldrich GmbH, Vienna, Austria) and spun down, and subsequently, RNA was isolated using a Favorprep™ Tissue Total RNA Purification Mini Kit (Favorgen, Taipei, Taiwan). The synthesis of the complementary DNA (cDNA) was performed with a QuantiTect Reverse Transcription Kit (QIAGEN Inc., Valencia, CA, USA). Gene expression levels of *ICAM1*, *VCAM1,* and platelet endothelial cell adhesion molecule 1 (*PECAM1*) were evaluated with a 7500 real-time PCR system (Thermo Fisher Scientific, Vienna, Austria). The sequences of all primers are shown in Table 2.

### 2.11. Evaluation of inflammatory behavior utilizing primary macrophage cells

The influence of hpcECM coating on the expression of pan-, pro- and anti-inflammatory macrophages (CD68, CCR7, CD80, CD163, and CD206) and cytokines (IL-1α, TNF-α, and IL-10) was studied using qPCR. To do so, human PBMCs were isolated from three donors and differentiated into macrophages.[39] Subsequently, the macrophages were seeded on the uncoated, 0.02% and 0.2% hpcECM-coated PCL patches ($5 \times 10^5$ cells/well) in 24-well plates ($n = 6$, derived from 3 donors) for 1, 3, and 7 days. Total cellular RNA was isolated using the RNeasy Mini Kit via the QIAcube system (both from Qiagen, Valencia, CA, USA). Reverse transcription was performed using the Go–ScriptTM Reverse Transcription System (Promega GmbH, Vienna, Austria). Finally, the real-time PCR was performed with a Roche light cycler 480 (Roche AG, Basel, Switzerland). Briefly, the Ficoll separation method was used for the isolation of PBMCs (same protocol as described in **Section 2.8**).

Isolated PBMCs were re-suspended in RPMI 1640 with 10% FBS (Millipore, Darmstadt, Germany) and seeded on tissue culture plates. Macrophage colony-stimulating factor (M-CSF) was added to the PBMCs for 5 days till they were differentiated into macrophages. Non-adherent cells were removed by washing the plates with PBS after 2 hours. Uncoated PCL constructs served as controls. All of the primers used in this study are shown in Table 2.

### 2.12. Statistical analysis

All data are expressed as mean ± standard deviation (SD). Statistical analyses were performed using GraphPad Prism software (Version 9.5.1, GraphPad Software Inc., CA, USA). The normal distribution of data was tested with the Shapiro–Wilk test. Based on the distribution of the data, unpaired *t*-test, one-way analysis of variance (ANOVA), or two-way (ANOVA) were applied. In detail, post hoc tests were conducted as multiple comparisons using either Sidak's or Tukey's test according to the distribution of the data. The Kruskal–Wallis test one-way analysis of variance (ANOVA) was employed to assess differences between the

**Table 2. Primer sequences.**

| Gene | Forward (5' to 3') | Reverse (5' to 3') |
|---|---|---|
| *CCR7* | GCTGGTCTGAGCATTTGAGT | CCAGAAACTGTTCCCACCTG |
| *CD68* | CCTGGGTTGCTAACCATCTCC | CCAGTGCTCTCTGTAACCGT |
| *CD80* | CGGGAAACACTGCTAGTACC | AAAGCCTTTAGAGCCAGCCC |
| *CD163* | CTCCTTACTCTCCTGATGCCAA | TGAAGACTCTGGATCTGCTGGT |
| *CD206* | CTTAGTTCCGCCCTCCTGTC | TGCCTCAGAGCAGACTTACC |
| *GAPDH* | GGAAGGAAATGAATGGGCAG | CCCAATACGACCAAATCAGAG |
| *ICAM1* | ATGCCCAGACATCTGTGTCC | GGGGTCTCTATGCCCAACAA |
| *IL1A* | CAGTGGTCTCATGGTTGTCA | CTTGAGCCAGTAATTGGTCCG |
| *IL10* | CTCAGCACTGCTCTGTTGCCT | AGCTGTTCTCAGACTGGGTGC |
| *PECAM1* | GCAACACAGTCCAGATATCG | GAC CTC AAA CTG GGC ATC AT |
| *TNFA* | TCGGGCCGACTATCTCGACT | CGTCCTCCTCACAGGGCAAT |
| *VCAM1* | GGGAAGATGGTCGTGATCCTT | TCTGGGGTGGTCTCGATTTTA |

three coating groups. In the case of a significant Kruskal–Wallis test, Dunn's test with Bonferroni correction was performed pairwise between specific pooled groups. Also, statistical significance was set at $p < 0.05$ for all statistical tests.

## 3. Results and discussion

### 3.1. 3D printing process and characterization of hpcECM

Material selection, architecture, and mechanical characteristics of the patch are prerequisites for sufficient integration of the patch into the anatomy of the heart for providing adequate mechanical and regenerative support. At the macro scale, the geometry and morphology of the patch are important parameters, whereas, at the microscale, the complex 3D architecture of the scaffold determines the prerequisites for cell migration and proliferation, vascularization, and nutrient, metabolite, and oxygen diffusion.[40,41] The biodegradable PCL patches were printed in three steps with a 3D-Bioplotter through a pneumatic extrusion technique. The first layer provided vertical lines (strand width of 266.136 ± 3.461 µm, printing speed: 16 mm/s), covered by a second layer consisting of oval-shaped pores with various ellipsis aspect ratios (major axis/minor axis of the oval, strand width 423.178 ± 17.760 µm) (Figure 1a–c and 1e). The surface of the strands represented micro-pores (Figure 1d). The printing parameters such as printing temperature, speed, pressure, and platform temperature were precisely optimized (Table 1). In this study, the major focus was to enhance cardiac-specific cell adhesion and proliferation on an extremely hydrophobic thin patch, which typically has limited available surface for cell attachment. The geometry of the studied patch had large pores with relatively thin strand width, representing a suitable model with restricted available surface for cell attachment.

3D-printed patches were subsequently coated with human placenta chorion ECM. The decellularization process of the chorion membrane and the quality of the produced hpcECM hydrogel were examined for each batch. H&E staining of the decellularized samples showed the structural integrity of the ECM protein network[42] and revealed complete cell component removal (Figure 1f and 1g). DNA content was reduced significantly (99.99975%) with average DNA residues of 4064.50 ± 44.56 ng/mg dry weight for native and 1.00 ± 0.03 ng/mg dry weight for decellularized samples (DNA removal efficiency: 99.99975%). Since this residual amount is less than 50 ng double-stranded DNA (dsDNA) per mg dry weight, this product is considered a safe hydrogel in terms of causing an immune reaction after application.[43] The macromolecule composition of the ECM proteins is substantial for cell adhesion, differentiation, and migration.[44] Therefore, the post-decellularization content of ECM proteins was evaluated. The collagen content of native (157.11 ± 17.97 µg/mg) and decellularized tissue (243.06 ± 26.22 µg/mg dry weight) was preserved considerably. The increase in collagen content is due to normalization of values to the dry weight of the samples, this reflects the loss of cell mass and soluble proteins in the tissue.[34,45] Elastin content showed no significant reduction (native: 1.43 ± 0.09 µg/mg dry weight; decellularized: 1.36 ± 0.14 µg/mg dry weight). GAG quantification showed 75% preservation of GAG content (native: 1.15 ± 0.05 µg/mg dry weight, decellularized: 0.87 ± 0.04 µg/mg dry weight) The protein composition analyses confirmed a successful decellularization process, with the preservation of protein structure (Figure 1h–k).

### 3.2. Surface and mechanical characterizations

Mechanical stiffness and topographical characteristics of the cellular 3D environment have a tremendous influence on the fate of cells in terms of adhesion, migration, proliferation, and even differentiation. Cells actively examine and adopt their pericellular space to fit their requirements. This is a bi-directional interchange between the characteristics of the 3D extracellular environment and their own secreted pericellular medium.[46] For instance, cells are capable of sensing and probing the micro stiffness of the surrounding and degrading the ECM matrix to regulate their fate in a dynamic manner.[47] In regard to the dynamic nature of the biological process, biodegradable polymers, and hydrogels in *in vitro* settings can be contemplated as initial examples of dynamic procedures, where the integrity and stiffness progressively decline with time via hydrolysis or enzymatic degradation.[48]

The influence of hpcECM coating on the surface and mechanical characteristics of the biodegradable patch were assessed via pore size, porosity, nanoindentation, unidirectional tensile strain, wettability, surface topography and roughness studies. However, the first critical step was to confirm the successful coating process and validate the method of the coating in 0.02% and 0.2% hpcECM hydrogel-coated samples. Initially, SEM was utilized to visualize the coating. SEM images of the 0.02% hpcECM-PCL, 0.2% hpcECM-PCL, and uncoated PCL samples are shown in Figure 2a and 2b. The coating could not be detected via SEM imaging due to the very low concentration of the utilized hydrogel and therefore possible creation of an extremely thin layer of ECM on the surface. Next, the immunofluorescence staining method was utilized to visualize the coating. It was previously shown that laminin and fibronectin were successfully preserved in the hpcECM gel after the decellularization process.[35] Therefore, coating visualization was examined via immunofluorescence staining of fibronectin. Samples

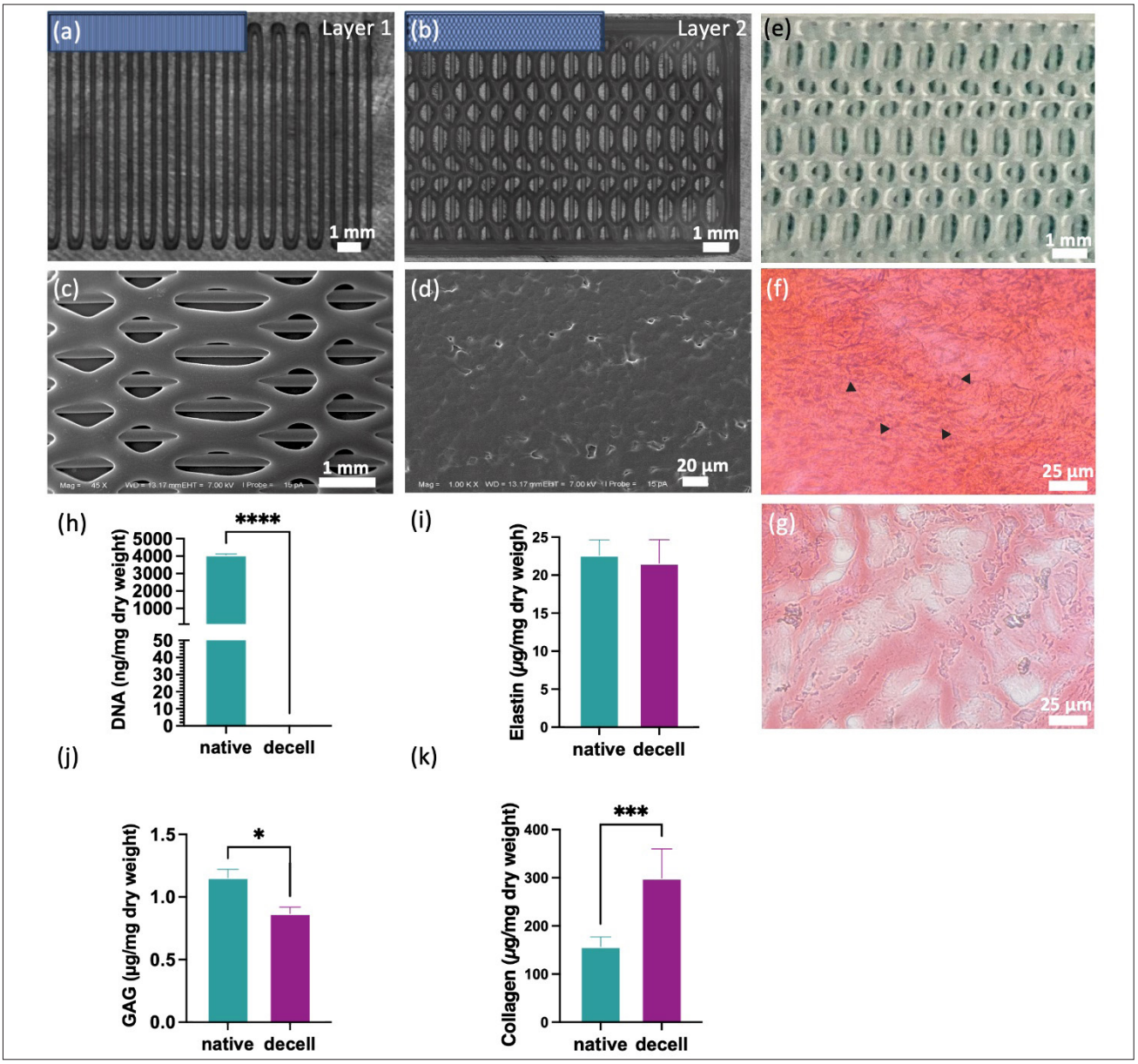


**Figure 1.** 3D printing fabrication process and material development via decellularization. The utilization of 3D printing provided an accurate control of PCL deposition for the fabrication of a patch with large pores. (a, b) structure of the 3D-printed layers. (c–e) SEM micrographs of the patch: (c) macrostructure, (d) microstructure (surface topography), and (e) prototype printed patch. Characterization of ECM hydrogel confirmed a successful decellularization and production of human placenta chorion ECM hydrogel. (f, g) H&E stained images confirmed the absence of cells after decellularization: (f) native chorion, and (g) decellularized chorion (arrows show the native cells in the native tissue). (h) DNA content was significantly reduced in the decellularized tissues compared to the native tissues (****$p < 0.0001$, 99.9997%). (i–k) The amount of (i) elastin, (j) GAG, and (k) collagen preserved in the decellularized tissue ($n = 4$). Abbreviations: GAG: Glycosaminoglycans; H&E: Hematoxylin and eosin; hpcECM: Human chorion placenta extracellular matrix; PCL: Poly-ε-caprolactone; SEM: Scanning electron microscopy.

coated with 0.02% (2 mg/mL) and 0.1% (1 mg/mL) fibronectin served as controls. Fibronectin has previously shown great potential in supporting re-endothelialization of polymeric grafts as a coating agent and reducing fibrosis with low immunogenicity leading to cardiac repair as a cardiac patch.[17,49] In terms of optimization of the method, samples incubated for 2 hours in coating solution were compared with samples incubated for 72 hours. Uncoated samples showed no signal, proofing the lack of background signals. A thin layer of positive staining was present in all coated samples (Figure 2e). In general, increasing the incubation time from 2 to 72 hours slightly increased the

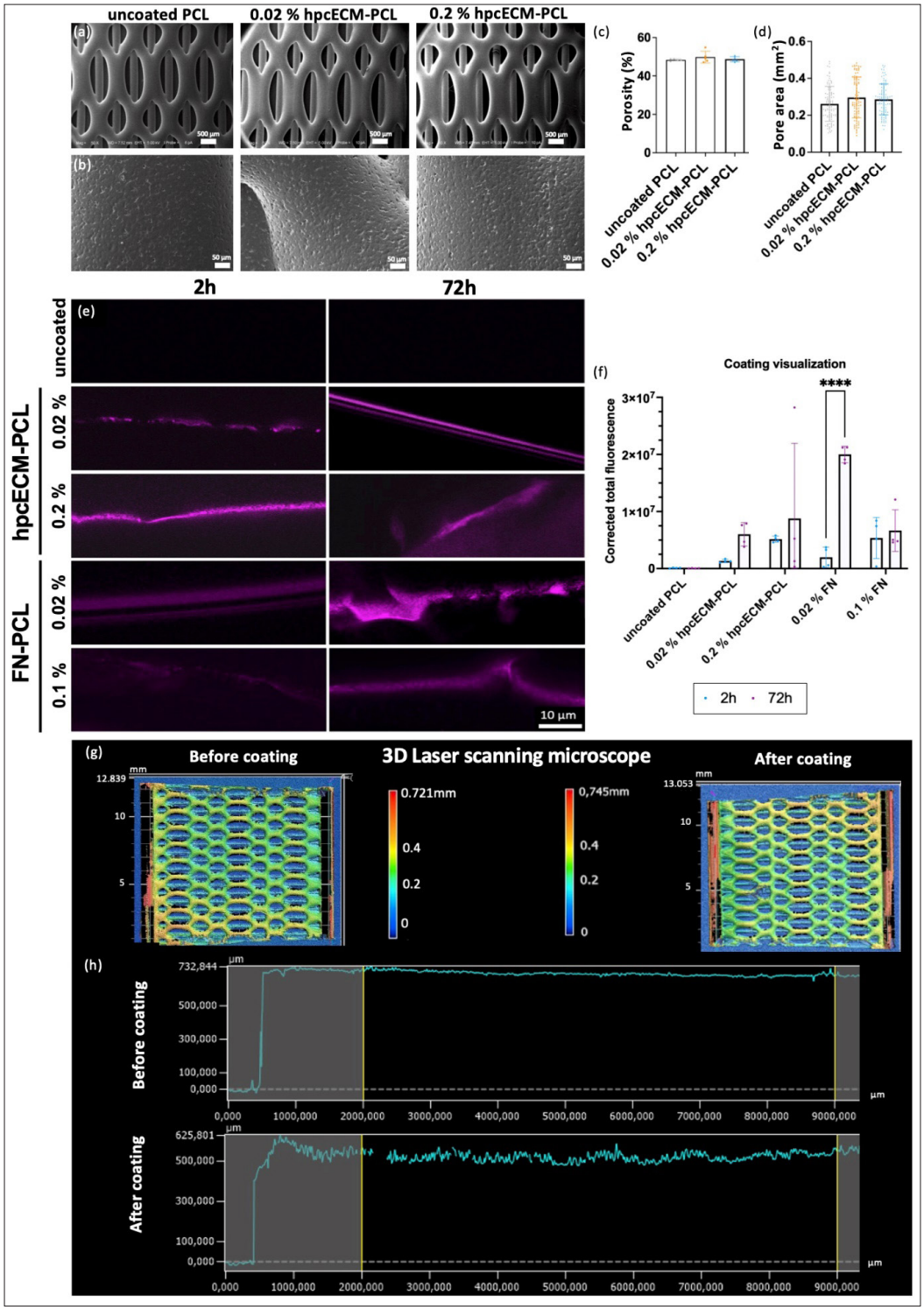


**Figure 2**. Scanning electron microscopy, porosity, pore size, coating visualization, 3D optical microscanner/profilometer results. (a, b) SEM images of coated and uncoated samples in two different magnifications: _50_× in (a); _500_× in (b). (c) Porosity, (d) pore size, (e) fibronectin immunofluorescence staining of the samples, with the fibronectin signal detected in both hpcECM- and fibronectin-coated samples. (f) Quantification of coating efficiency and influence of incubation time on coating; no significant differences were observed between the groups (except for samples coated with less concentration of fibronectin) (****$p < 0.0001$). (g, h) Results from 3D optical profilometer: (g) surface height profile, and (h) roughness profile and quantifications measured by VR-5200 wide-area 3D optical profilometer. The presence of hpcECM caused a smoother surface inducing a decline in surface roughness. Abbreviations: FN: Fibronectin; hpcECM: Human chorion placenta extracellular matrix; PCL: Poly-ε-caprolactone; SEM: Scanning electron microscopy.

efficiency of coating (Figure 2f). However, this was only significant in 0.02% of fibronectin-coated samples. The coating efficiency with lower fibronectin concentration increases with incubation time.

Furthermore, pore size and porosity were studied (Figure 2c and 2d). The mean pore size distribution of the uncoated PCL samples, 0.02% hpcECM-PCL, and 0.2% hpcECM-PCL was 0.26 ± 0.09, 0.31 ± 0.12, and 0.29 ± 0.09 $mm^2$, respectively. The large standard deviation is attributed to the existence of two different pore size categories (large and small ones) in the patch design. The porosity of the uncoated PCL samples, 0.02% hpcECM-PCL, and 0.2% hpcECM-PCL was 48.34 ± 0.01%, 48.74% ± 0.01%, and 49.79 ± 0.03%, respectively. In general, coating did not show any significant effect on the pore size distribution and porosity. The pneumatic extrusion technique provided high reproducibility and precise control over the pore size, shape, and pore size distribution.

The surface profile and the roughness of the patches before and after coating were further studied via a 3D optical microscanner/profilometer. An example of the surface profile of a sample coated with 0.02% hpcECM hydrogel is shown in Figure 2g. The surface color coding and height of the patches before and after coating changed slightly. This indicates the presence and distribution of the hpcECM coating on the porous material. Further quantifications were applied to measure the surface roughness, a factor that also influences cell attachment. Increased surface roughness has been shown to increase cell adhesion on polymers.[50] 3D-printed patches had micropores on the surface providing a relatively rough surface; however, the addition of a thin hpcECM hydrogel layer led to a smoother surface and the average roughness decreased from 13.9 µm to 5.9 µm in 0.02% hpcECM-PCL (57% decrease) and from 15.0 µm to 5.3 µm in 0.2% hpcECM-PCL (64.6% decrease) (Table 3, Figure 2h). This could translate to less potential in cell adhesion; however, it should be noted that surface wettability is another critical factor that could compensate for the low surface roughness.

Contact angle measurements and FSE measurements could give us an insight to the degree of hydrophobicity of the uncoated PCL and hpcECM-coated samples (Figure 3a–d). In this study, porous 3D-printed samples were compared with an identical 3D-printed flat nonporous PCL structure, in order to additionally investigate the role of porosity in the coating process.

Both flat and porous samples showed a very significant reduction in contact angles between coated and uncoated groups ($p < 0.0001$), confirming the role of hpcECM in inducing surface hydrophilicity to the hydrophobic biopolymer. In contrast to the flat samples, there were no significant differences between the samples coated with 0.2% and 0.02% hpcECM in porous samples. This could be due to the fast absorption of the droplet on the porous samples causing challenges in contact angle measurements and leading to a higher SD (Figure 3b and 3c). Furthermore, FSE data showed that the more concentrated hpcECM could provide high surface energy, suggesting the higher hydrophilicity (0.2% hpcECM-PCL: 58 mN/m, 0.02% hpcECM-PCL: 41 mN/m, uncoated PCL: 31 mN/m) (Figure 3d). Additionally, clear differences regarding the shape of the droplet on the surface of the samples were apparent (Figure 3a). In aliphatic polyesters such as PCL, the presence of hydrocarbon backbones induces low hydrophilicity, which limits cell spreading and therefore ECM formation.[51] However, in our study, the hpcECM hydrogel coating could provide a hydrophilic layer consisting of fundamental constituents of the ECM. This thin layer of ECM hydrogel could support a range of biomimetic systems leading to a higher moiety and induced interaction between cells and biomaterials. Furthermore, the mechanical characteristics of the 0.02% hpcECM-PCL, 0.2% hpcECM-PCL and uncoated PCL patches were analyzed via unidirectional tensile strain measurements (Figure 3e–h). The ultimate tensile strength (UTS), strain at failure (SAF), and modulus of E of the uncoated patch were 3.59 ± 0.4 Mpa, 11.84% ± 2.8% MPa, and 31.78 ± 7.3 Mpa, respectively. No significant differences were

**Table 3. Roughness profile and quantifications measured by 3D optical profilometer.**

| Sample | Ra Avg. (µm) | Ra Max. (µm) | Ra Min. (µm) | SD (µm) |
|---|---|---|---|---|
| Uncoated $PCL_1$ | 13.99 | 28.24 | 6.87 | 6.80 |
| 0.02 % hpcECM-$PCL_1$ | 5.93 | 14.97 | 1.80 | 4.35 |
| Uncoated $PCL_2$ | 15.03 | 39.30 | 2.64 | 11.78 |
| 0.2 % hpcECM-$PCL_2$ | 5.37 | 11.99 | 2.32 | 3.31 |

Notes: $PCL_1$: PCL patch group one, Samples in group one were coated with 0.02% hpcECM-PCL; $PCL_2$: PCL patch group two, Samples in group two were coated with 0.2% hpcECM-PCL.

Abbreviations: hpcECM: Human chorion placenta extracellular matrix; PCL: Poly-ε-caprolactone; Ra Avg.: Average roughness; Ra Max.: Maximum roughness; Ra Min.: Minimum roughness; SD: Standard deviation.

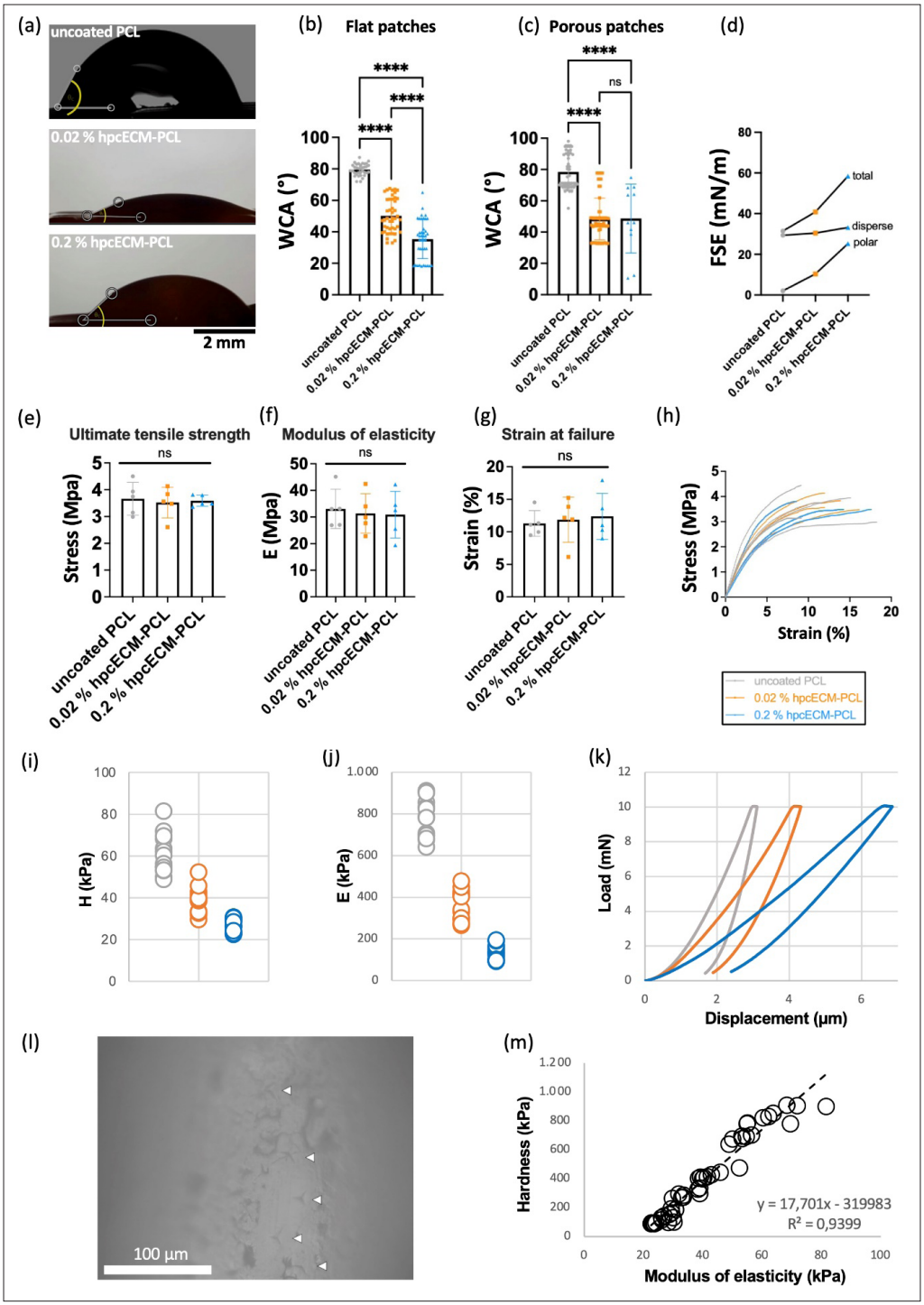


**Figure 3**. Wettability analysis, mechanical characterization via unidirectional tensile strain, and nano-indentation measurements. (a–c) Wettability and contact angle measurements of flat vs porous samples. (d) Free surface energy (FSE) characterization; polar, dispersed, and total FSE based on different hpcECM concentrations. A higher FSE indicates a more hydrophilic surface. Increased hydrophilic properties with increasing hpcECM concentration were observed. (e–h) Unidirectional tensile strain measurements: (e) ultimate tensile strength (UTS), (f) modulus of elasticity (E), (g) strain at failure (SAF), and (h) stress-strain curve. (i–l) Results pertaining to nanoindentation: (i) indentation hardness; (j) indentation modulus of elasticity; (k) typical load-displacement curves from nanoindentations, showing that hpcECM provided a softer and more elastic environment at the cellular level; (l) image showing indentation positions on the surface (indicated by white arrows). (m) Correlation between indentation hardness and indentation modulus confirmed the high accuracy of the gel mechanical characterization method at the nanoscale level. Abbreviations: hpcECM: Human chorion placenta extracellular matrix; PCL: Poly-ε-caprolactone.

**Table 4. Mechanical characteristics via nanoindentation and unidirectional tensile strain measurements.**

| Sample | $H_{IT}$ (MPa) | $E_{IT}$ (MPa) | UTS (MPa) | SAF (%) | E (MPa) |
|---|---|---|---|---|---|
| Uncoated PCL | 0.06 ± 0.08 | 0.77 ± 0.08 | 3.66 ± 0.61 | 11.29 ± 1.96 | 33.07 ± 7.40 |
| 0.02% hpcECM-PCL | 0.03 ± 0.05 | 0.35 ± 0.07 | 3.59 ± 0.20 | 12.38 ± 3.53 | 30.9 ± 8.73 |
| 0.2% hpcECM-PCL | 0.02 ± 0.01 | 0.12 ± 0.03 | 3.52 ± 0.57 | 11.86 ± 3.47 | 31.37 ± 7.38 |

Abbreviations: E: Modulus of elasticity; $E_{IT}$: Indentation modulus; $H_{IT}$: Indentation hardness; hpcECM: Human chorion placenta extracellular matrix; PCL: Poly-ε-caprolactone; SFA: Strain at failure; UTS: Ultimate tensile strength.

observed in the stress-strain response between the coated and uncoated groups at the macroscopic level (Figure 3h). The mechanical characteristics of cardiac tissues vary between systolic and diastolic phases, with infarcted tissue exhibiting even significantly greater stiffness. For instance, the modulus of elasticity of human cardiac tissue differs from 0.02 to 0.50 MPa. Furthermore, the UTS and the SAF are in the ranges of 3–15 kPa and 22–90%, respectively. This wide range highlights the challenge of defining optimal mechanical properties for related applications.[40,52] In general, the hpcECM-PCL patch was stiffer compared to the cardiac tissue and the bulk modulus of elasticity of the patches was significantly higher than that reported for the native human cardiac tissue. However, it has been shown previously that even much stiffer cardiac patches could induce an improved outcome in terms of inhibiting unwanted pathophysiological remodeling and boosting cardiac regeneration by preventing further damage to cardiomyocytes.[52] This has been additionally confirmed by Wall et al.[53] in a theoretical simulation model. Considering that a very stiff patch may lead to diastolic dysfunction, Wall et al. showed that patches significantly stiffer than cardiac muscle are preferable to matrices with higher elasticity. This might be due to the fact that stiffer patches could more effectively reduce cardiac wall stress.

At the microscopic level, nanoindentation showed that the modulus of elasticity ($E_{IT}$) of the surface (hpcECM) and the indentation hardness ($H_{IT}$; force divided by contact area under load) decreased with increasing hpcECM concentration ($p < 0.001$) (Figure 3i–k, Table 4). All this confirms that the coating could provide a mechanically softer microenvironment for the cells, which might potentially support the mechanosensitive signaling pathways.[54,55] Pooling the data resulted in a strong correlation ($R^2$ = 0.940) between the hardness and modulus of elasticity. The indentation positions on the surface are shown in Figure 3l. The position of Pooling the data resulted in a strong correlation ($R^2$ = 0.940) between the hardness and modulus of elasticity (Figure 3m).

This confirms the accuracy of the measurement in micro/nano-scale. Since the ECM gel contains more than 40% collagen (mainly type I and III collagen),[35] this component could have a substantial role in defining the mechanics/stiffness of the constructs. Collagen fibrils present a stiffness ranging from 300 MPa to 1.2 GPa.[56] However, the stiffness of a reconstituted collagen type I gel could drop down to tens or hundreds of Pascals in both micro- and macro-scales.[57] Kolliopoulos et al.[58] have shown that introducing the chorion extracts to a mineralized collagen matrix could reduce the stiffness from 1.5 MP to less than 0.5 MPa. In this study, macro mechanical (unidirectional tensile strain) and micromechanical (nano-indentation) measurements suggest that the PCL 3D-printed construct with high UTS, and high modulus of elasticity is responsible for the bulk mechanical behavior of the patch, whereas hpcECM with a lower modulus of elasticity provides a soft microenvironment for cell adhesion and proliferation comparable to cardiac tissue in microscale.

### 3.3. Biocompatibility, cell attachment and hemocompatibility assessment

Various cell types, apart from cardiomyocytes, are involved in remodeling during cardiac regeneration. Endothelial cells and fibroblasts both play crucial roles in maintaining tissue function and homeostasis. Fibroblasts are the main production source of the extracellular matrix (ECM) with high type 1 collagen and fibronectin content.[59] The activation and migration of fibroblast cells are crucial for physiological processes related to angiogenesis. They have the capability to induce the formation of capillary-formed structures in the presence of endothelial cells.[59,60] Likewise, endothelial cells have substantial angiogenic characteristics in addition to the capability to transdifferentiate into cardiac muscle tissue.[61]

Here, primarily, the cell viability and proliferation of fibroblasts and endothelial cells were studied and compared by utilizing both HFFs and HUVECs. Live/dead staining of the HFFs and relevant SEM images revealed that all three groups of uncoated and coated PCL induced no cytotoxic effects. However, the patches coated with higher concentration of ECM supported the HFF cell proliferation more and cells presented a more elongated morphology in the dense populations (Figure 4a and 4b). XTT assay

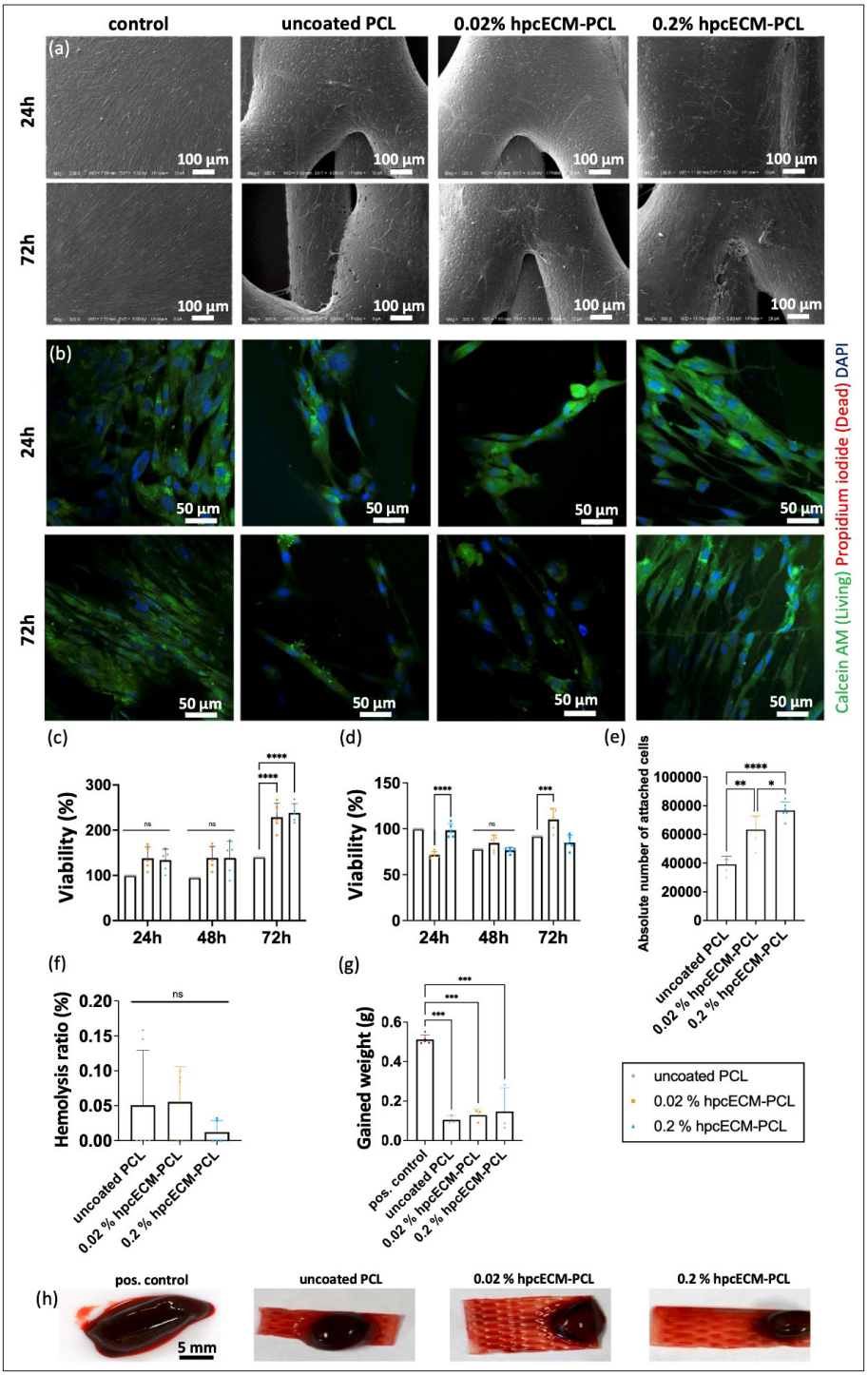


**Figure 4.** Biocompatibility, cell attachment, and hemocompatibility assays. (a) SEM images and (b) live/dead staining of patches cultured with HFFs for 24 and 72 hours. Patches significantly supported cell attachment. Most of the cells were viable (green cells) and only a limited number of cells were dead (almost no red cells). Both hpcECM-coated PCL samples supported cell proliferation significantly. (c–d) Determination of HFFs and HUVECs proliferation on coated and uncoated samples via XTT assay. Coating with hpcECM increased HFF proliferation after 48 and 72 hours. (e) Cell attachment assay revealed an evident, significant increase of HUVECs' initial attachment in coated samples 30 min after seeding. (f) Hemolysis ratio of tested samples. (g, h) Blood clot formation assay. Blood clot formation was significantly lower in the specimens than in the positive control. No significant difference in clot weight was detectable between coated and uncoated samples; in other words, the tested groups did not induce hemolysis. Abbreviations: HFFs: Human foreskin fibroblasts; hpcECM: Human chorion placenta extracellular matrix; HUVECs: Human umbilical vein endothelial cells; PCL: Poly-ε-caprolactone; SEM: Scanning electron microscopy.

confirmed that first the uncoated PCL patch along with the hpcECM-coated samples were biocompatible, and they did not show any cytotoxicity effect on both HUVECs and HFFs, which proliferated continuously within 24, 48, and 72 hours (Figure 4c and 4d). However, HFFs seeded on 0.2% and 0.02% hpcECM-coated samples promoted the proliferation significantly more than the uncoated groups. This confirms the capability of hpcECM to provide cells with an environment with higher cell affinity, promoting the proliferation and metabolic activity of the cells. The initial cell attachment assay confirmed significant improvement in HUVECs attachment in the coated patches after 30 min of seeding (Figure 4e). Afterward, the proliferations were promoted mainly in 0.02% hpcECM-coated groups after 72 hours (Figure 4d).

The difference in proliferation rate between various cell types was observed during the myocardial infarct repair process.[62] This could be due to the fact that, in general, fibroblasts are constantly producing ECM and they effectively generate their individual preferable environment that promotes growth and proliferation.[63] Myofibroblasts and endothelial cells proliferate and migrate into the infarct region, and they attempt to substitute the necrotic tissue with provisional granulation tissue. It has been shown that the proliferation of myofibroblasts is around 5% higher compared to endothelial cells at the beginning of the repair process.[62] However, as repair progressed, the proliferation rate of both cell types decreased but the trend stayed similar.[62] Furthermore, fibroblasts support and modulate endothelial migration and proliferation in various spheroid co-culture setups.[64]

Hemocompatibility of the PCL patches coated with 0.2% and 0.02% hpcECM was assessed via blood clot formation and hemolysis assays in a static set-up (Figure 4f–h). Figure 4h shows the actual thrombus formed in the presence of the patches. Results revealed that there were significant differences between the positive control and all other coated and uncoated PCL batches. HpcECM coating by itself did not induce any significant alteration in terms of the formed thrombus weight (uncoated PCL: 0.105 ± 0.016; 0.02% hpcECM-PCL: 0.129 ± 0.023; 0.2% hpcECM-PCL: 0.147 ± 0.077; Figure 4g). However, this assay is capable of providing an estimation regarding the hemocompatibility of the uncoated and coated patches. Hemolysis assay provided a more precise assessment in terms of studying the degree of red blood cells (RBCs) destruction induced by the PCL and hpcECM materials. All coated and uncoated groups showed a very low hemolysis rate (all data are below 0.5%, threshold of the hemolysis in humans is approximately 10%),[65] confirming the non-hemolytic characteristics of the pure PCL and the ECM coating (Figure 4f).

### 3.4. EPCs attachment and adhesion molecule expression

EPCs are circulating cells that contribute to vascular and cardiac repair.[66] They could adhere to the endothelium in ischemic regions in the myocardium and participate in vascularization of the tissue, modulation of immune response and ECM deposition, promoting cardiac microenvironment development.[67,68] In our study, the adhesion of the EPCs to the hydrophobic patches and the role of hpcECM in promoting an endothelial layer were investigated. To do so, freshly isolated EPCs were cultivated on the uncoated PCL and coated patches (0.02% hpcECM-PCL and 0.2% hpcECM-PCL). Fibronectin-coated samples served as controls. It has previously been shown that fibronectin alone or in combination with other ECM proteins such as collagen, elastin, and laminin (in the form of either protein or bifunctional peptide) could support endothelialization.[69-71]

Figure 5a and 5c show that prominin-1 (Prom-1) positive cells were detectable after one week. It was shown that significantly less EPCs attached to fibronectin and uncoated samples (Figure 5b). Furthermore, all attached cells were counted (Prom-1+ and Prom-1- cells) and uncoated samples showed the lowest level of Prom-1 compared with hpcECM and fibronectin coated samples(Figure 5c). This could potentially indicate an increased EPCs recruitment on the coated samples and higher crosstalk between EPCs and other cardiac cell populations such as ECs and cardiac fibroblasts. Furthermore, the influence of hpcECM on the expression level of some key cell adhesion molecules, namely ICAM-1, VCAM-1, and PECAM-1, was further studied (Figure 5d). ICAM-1 and VCAM-1 facilitate inflammation and promote leukocyte migration in an inflammatory state.[72] Further, they support forming endothelial barriers while providing structural support and a binding platform for ECM components. PECAM-1 plays a main role in restoring the vascular permeability barrier following the endothelial cell junction disorder.[73]

Our study demonstrated no significant influence in the expression of ICAM-1, VCAM-1, and PECAM-1 in both the hpcECM-coated and uncoated groups. This absence of ICAM-1 and VCAM-1 overexpression in hpcECM could highlight the role of the hpcECM hydrogel in hindering leukocyte adherence to endothelial cells in an inflammatory state.[72] These findings are in conformance with the results of previous studies[35,74] showing that adhesion and growth of endothelial cells could be promoted without raising the expression of inflammatory cytokines (ICAM-1 and VCAM-1) and selectins. The enhanced adhesion of endothelial cells was complemented by substantial volumetric enlargement of the cells and a prominent

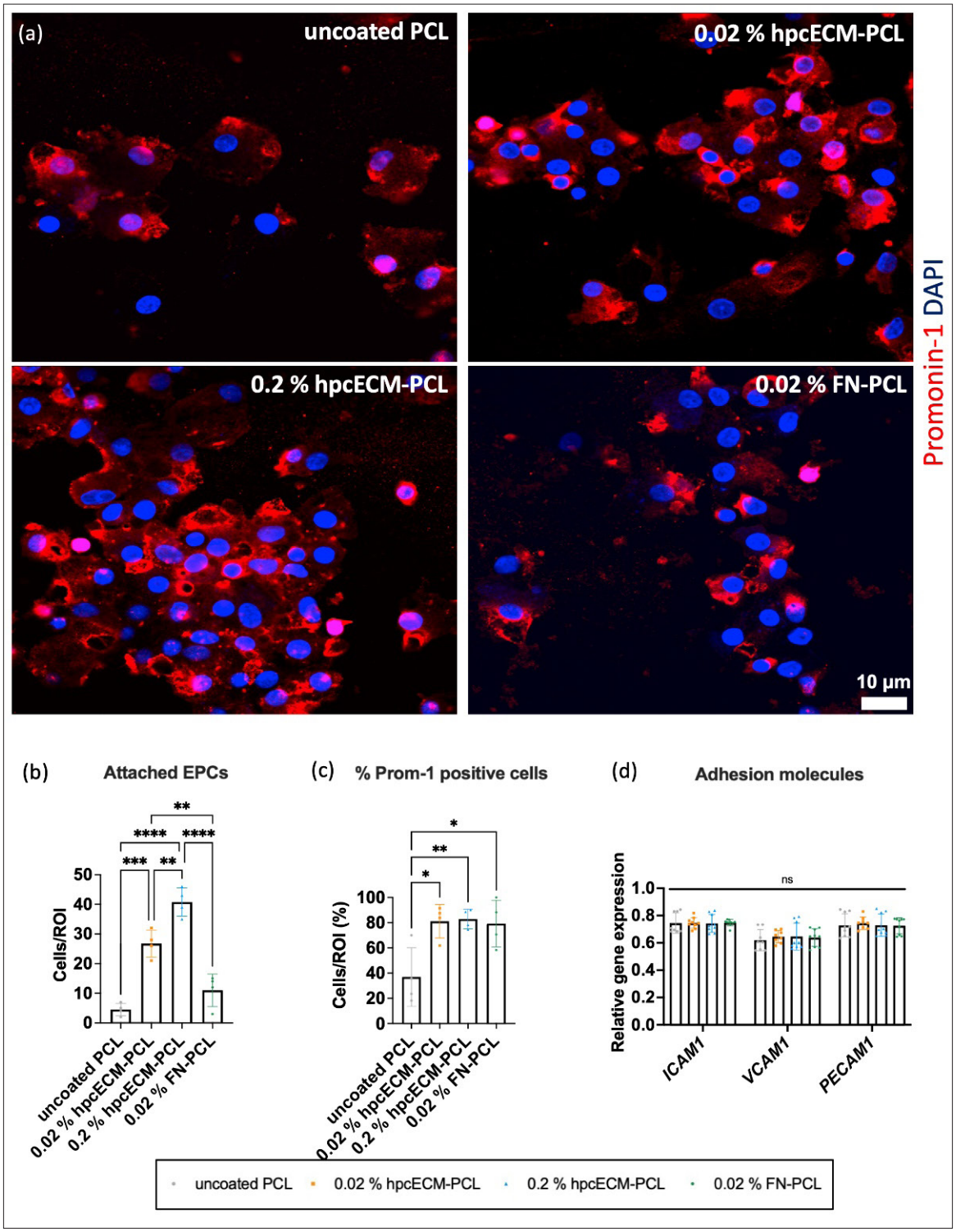


**Figure 5**. Attachment of endothelial progenitor cells and the activation and gene expression of adhesion molecules. (a, b) The presence of hpcECM coating significantly supported EPCs attachment compared to uncoated and fibronectin-coated patches. (c) The number of Prom-1 positive cells confirmed the activated state of EPCs in both hpcECM- and fibronectin-coated groups. (d) *ICAM1, VCAM1, and PECAM1* gene expression levels showed no significant differences between the groups, implying the role of some other adhesion binding receptors such as integrins in promoting the endothelial cells adhesion. Abbreviations: EPCs: Endothelial progenitor cells; hpcECM: Human chorion placenta extracellular matrix; ICAM-1: Intercellular adhesion molecule 1; PCL: Poly-ε-caprolactone; PECAM-1: Platelet endothelial cell adhesion molecule 1; Prom-1: Prominin 1; VCAM-1: Vascular cell adhesion molecule 1.

presence of cytoskeletal vimentin. These play a substantial role in supporting intercellular contacts and endothelial monolayer integrity. All these could suggest the possible role of other proteins such as vimentin or integrins in cell binding to hpcECM, as integrin $\alpha_5\beta_1$ and $\alpha_v\beta_3$ could stabilize ECM and are mediators of EPCs adhesion to fibrin.[74,75]

### 3.5. Viability and proliferation of undifferentiated and retinoic acid-differentiated H9c2 cells

Cardiomyocytes, the muscle cells responsible for the contraction and relaxation, are the largest cell fraction by volume in heart. H9c2 cells are originally derived from embryonic rat ventricular tissue[76] and are currently used *in vitro* to mimic skeletal and cardiac muscle. H9c2 cells share abundant characteristics with primary cardiomyocytes, such as membrane morphology, G-protein signaling expression, and electrophysiological properties, although they have lost their ability to beat.[77]

Furthermore, it has been shown that the differentiation of H9c2 cells via RA induces a predominant presence of cell types with an adult cardiac muscle phenotype, characterized by the overexpression of cardiac proteins such as troponin I and troponin T.[78] This confirms that RA induces the differentiation of the H9c2 cells toward a more cardiac-like phenotype, involving mitochondrial function remodeling. However, the majority of recent studies have utilized undifferentiated H9c2 myoblasts, raising concerns regarding the significance and relevance of the obtained results when compared to primary cardiomyocytes.[78,79]

In this study, both undifferentiated and RA-differentiated H9c2 cells were cultivated on coated and uncoated PCL patches (0.02% hpcECM-PCL and 0.2% hpcECM-PCL). The successful differentiation procedure was confirmed via troponin T staining. RA-differentiated cells clearly expressed troponin T protein (red dots), which was however absent in undifferentiated cells (Figure 6b and 6f). The morphology of the cells was also shown via SEM images in Figure 6a and 6e. XTT assay and live/dead staining confirmed the role of hpcECM in supporting attachment and proliferation of the H9c2 cells in both differentiated and undifferentiated stage, but this was statistically significant only in the RA-differentiated cells after 72 hours in 0.2% hpcECM-PCL patches (Figure 6c, 6d, 6g, and 6h). This finding further confirmed the positive potential of hpcECM on the differentiation and proliferation of differentiated H9c2. Previously, it was shown that nano copper oxide-loaded gelatin as well as graphene oxide as a coating composite on a 3D-printed PCL cardiac scaffold could support H9c2 cell attachment after 24 hours. However, the proliferation of these cells at longer time points and the utilization of differentiated H9c2 cells remained unexplored.[40] Additionally, carboxymethyl cellulose (CMC)/gelatin)/graphene oxide-based 3D-printed cardiac scaffolds showed acceptable biocompatibility for H9c2 cells in the formulation with higher CMC concentration. However, this scaffold showed a 65% reduction in H9c2 cell viability compared to the control, confirming the sensitivity of these cells to the microenvironment and the superiority of the hpcECM compared to CMC.[80]

### 3.6. Inflammatory and immune modulatory potential assessment via primary peripheral blood macrophages

Macrophage polarization has a central role in orchestrating the immunomodulatory behavior of a bioconstruct. This behavior is defined by the activation state of the polarized macrophage, which includes classically activated pro-inflammatory (M1) and alternatively activated anti-inflammatory (M2) phenotype.[81] In this study, polarized expression levels of pro-inflammatory (CCR7, CD80, IL-1α, and TNF-α) and anti-inflammatory (CD163, CD206, and IL-10) macrophages and cytokine markers were assessed (Figure 7). A high donor-to-donor variability in mRNA levels was apparent as it was reported elsewhere.[81,82] In general, a moderate inflammatory gene expression was observed in all groups. In detail, slight pro-inflammatory gene expressions were shown in all groups at 24 hours and this was more significant at 72 hours. However, the expression of C-C chemokine receptor type 7 (CCR7) and CD80 decreased after 72 hours and this was significant in CCR7 expression between 72 hours and 1 week in 0.2% hpcECM groups (CCR7 vs CD206 expression on 0.2% hcpECM-PCL at 72h, $p = 0.02$; CCR7 expression on 0.2% hcpECM-PCL at 72 hours vs 1 week, $p = 0.0071$). After one week, a higher anti-inflammatory gene expression (CD163 and CD206) in both uncoated and in the 0.2% hpcECM groups was observed (Figure 7a). Regarding the cytokine expression levels, expression of tumor necrosis factor alpha (TNF-α) and interleukin (IL)-1 α were higher in the hpcECM-coated samples at 24 and 72 hours (with no statistical differences) (Figure 7b). This was in accordance with the previous findings of Kolliopoulos et al.[58] showing that chorion extract had a high level of cytokines, inducing an initial pro-inflammatory response. However, at later time points (1 week), a significant anti-inflammatory cytokine expression was induced by the 0.2% hpcECM group via high expression of IL-10 (IL-10 expression on PCL vs 0.02% hcpECM-PCL at 1 week, $p = 0.0107$). To conclude, a mild inflammatory reaction was shown in all samples. An initial pro-inflammatory response was induced in the chorion-coated samples. However, this proinflammatory expression declined and was compensated by a significant inflammatory expression of IL-10 in the 0.2% hpcECM groups after one week.

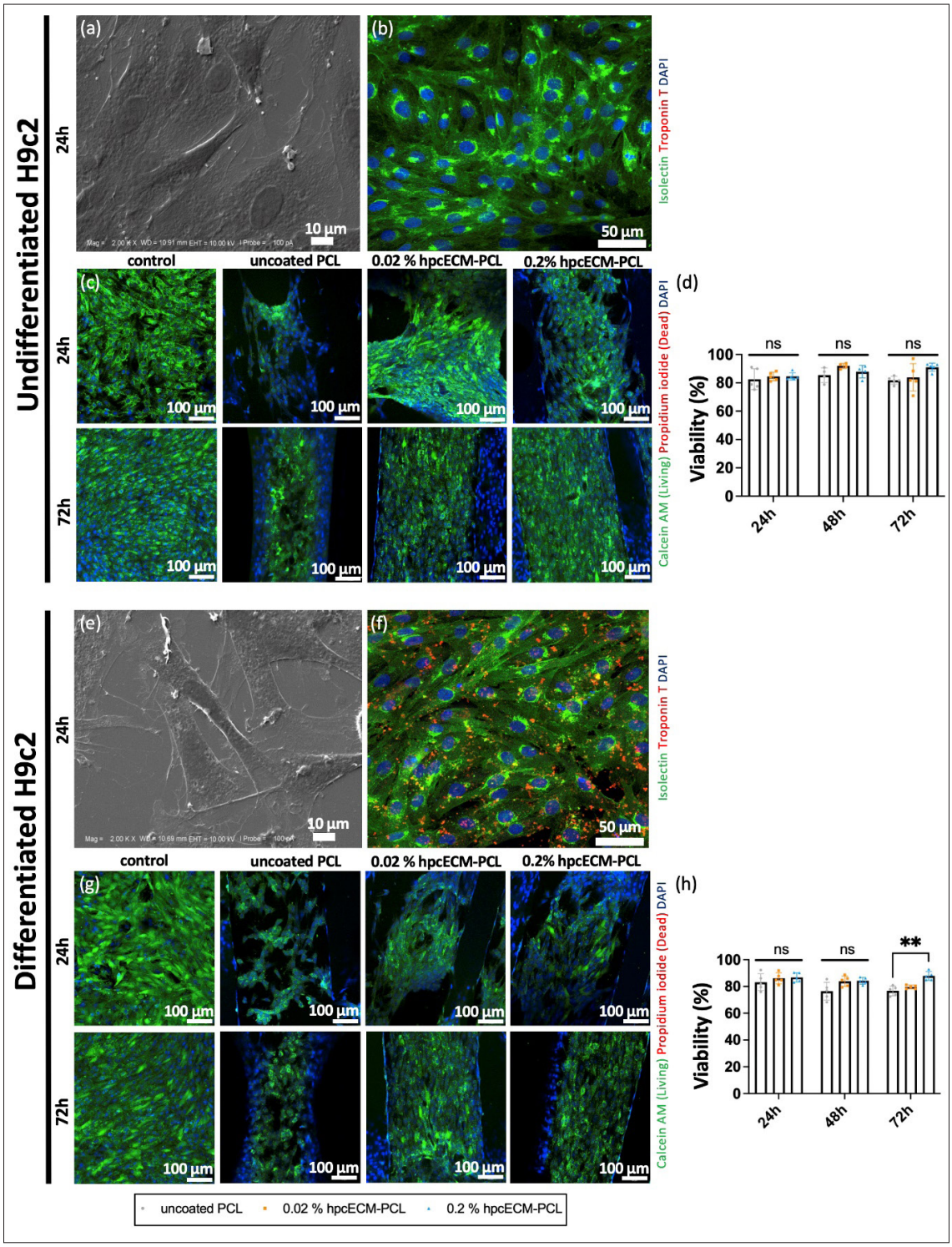


**Figure 6.** SEM, troponin T staining, live/dead staining and XTT assay of undifferentiated and RA-differentiated H9c2 cells. (a, e) SEM of the undifferentiated and differentiated H9c2 cells. (b, f) Troponin T staining confirmed the successful differentiation of H9c2 cells using RA. Differentiated cells clearly expressed troponin T (red dots). (c, g) Live dead (LD)-stained patches cultured with undifferentiated and RA-differentiated H9c2 cells for 24 and 72 hours. HpcECM clearly supported H9c2 cell attachment. Most cells were viable (green cells), whereas only some dead cells were detectable (almost no red cells). (d, h) Comparison of undifferentiated and RA-differentiated H9c2 cell proliferation on coated and uncoated samples detected by XTT assay. In general, hpcECM coating mainly increased proliferation specifically after 72 hours in RA-differentiated cells for the 0.2% hpcECM-PCL group. Abbreviations: hpcECM: Human chorion placenta extracellular matrix; PCL: Poly-ε-caprolactone; SEM: Scanning electron microscopy.

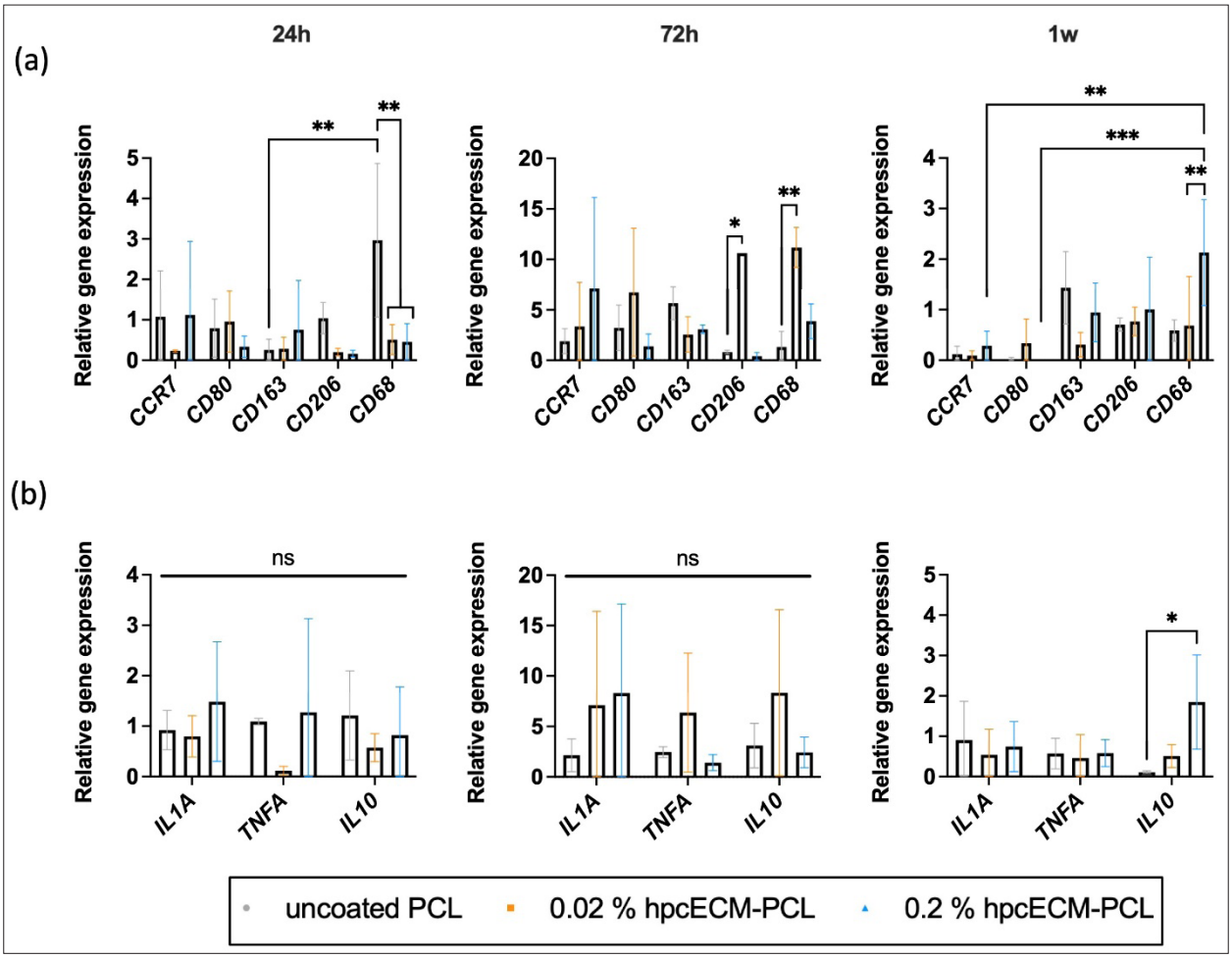


**Figure 7.** qPCR gene expression of anti-/pro-inflammatory macrophages *(CD68, CD80, CCR7, CD206, and CD163)* (a) and cytokine markers (*IL1A*, *TNFA* and *IL10*) (b) for the 0.2% hpcECM-PCL, 0.02% hpcECM-PCL and uncoated samples after 24 hours, 72 hours, and 1 week of cell culture. *GAPDH* was used as a housekeeping gene. Data are expressed mean ± standard deviation. $*p < 0.05$, $**p < 0.001$, $***p < 0.0001$. The graphs show $2^{-\Delta\Delta Ct}$ values of RT-qPCR runs performed on 6 samples derived from 3 donors. Error bars indicate 95% confidence intervals. Abbreviations: CCR7: Gene for C-C chemokine receptor type 7; hpcECM: Human chorion placenta extracellular matrix; *IL1A*: Gene for interleukin 1α; *IL10*: Gene for interleukin 10; PCL: Poly-ε-caprolactone; *TNFA*: Gene for tumor necrosis factor alpha.

### 3.7. Limitations and outlook

The current study demonstrated the positive influence of hpcECM on the adhesion and proliferation of cells on 3D-printed regeneration-supporting constructs. In general, ECM can regulate cell behavior through different mechanisms: (1) through direct cell-surface receptors and thus cell anchorage, or (2) via noncanonical growth factors and enzymes leading to the release of functional fragments.[83] Since a considerable amount of growth factors were not detectable in our hpcECM (data not shown), the second mechanism can be ruled out in future studies. Thus, further works on studying the mechanism of cell binding and identifying the activated receptors including ECM-integrin interaction will provide valuable insights.

ECM is considered a dynamic microenvironment for cardiac stem cells.[84] In this study, several cell types playing a critical role in cardiac repair such as endothelial cells, fibroblasts, EPCs, H9c2 undifferentiated and RA-differentiated cells, and macrophages were used. However, utilization of human induced pluripotent stem cells (hiPSCs) and investigation of hpcECM's ability to induce tissue-specific differentiation of hiPSCs to cardiomyocytes were not conducted in this study, warranting practical attempts in future works. Furthermore, functionality of these patches needs to be tested in an *in vivo* setting.

## 4. Conclusion

The developed hydrogel from human chorionic placenta (with high GAG, elastin and collagen content) is suitable as a cardiac cell-compatible coating agent for synthetic hydrophobic constructs due to its multiple excellent properties. The nanomechanical characterizations confirmed

the important role of hpcECM in providing a softer matrix with lower elastic modulus and hardness at the nanoscale, which has a positive effect on cell physiology. In addition, hpcECM could significantly promote the attachment and proliferation of important heart-related cells such as fibroblasts, endothelial cells, EPCs, and undifferentiated and RA-differentiated H9c2 cells. Our findings showed that the attachment of EPCs and the activation state of these cells were significantly improved, as indicated by the high expression of Prom-1. In addition, the differentiated H9c2 cells were able to proliferate significantly in more concentrated hpcECM (0.2%). HpcECM was able to convert early pro-inflammatory responses into anti-inflammatory responses after 1 week through high IL-10 expression. The results of this study indicate that compared to common coating agents such as fibrin used in cardiac regeneration, hpcECM is a successful candidate to enhance cardiac cell adhesion, proliferation and activation and to support the regeneration of extremely hydrophobic constructs.

## Acknowledgements

We would like to thank the personnel of the Department of Obstetrics and Gynaecology, MUW for the retrieval of placentas. Moreover, we appreciate the help of the Imaging Core Facility at the Medical University of Vienna. We also acknowledge the support of Dr Thomas Chudoba (ASMEC GmbH) for nanoindentation.

## Funding

This study was partly funded by the Ludwig Boltzmann Institute for Cardiovascular Research and by the Optiflow 3D project funded by the Austrian Research Promotion Agency (FFG) Nr. FO999891239.

## Conflict of interest

The authors declare that they have no known competing financial interests or personal relationships that could have appeared to influence the work reported in this paper.

## Author contributions

*Conceptualization:* Marjan Enayati, Karl H. Schneider, Helga Bergmeister

*Data curation:* Marjan Enayati, Christopher Riedmüller, Sabrina Rohringer, Felix Pointner, Luis Pichelkastner, Marta Bonora, Ewald Unger, Emir Benca

*Funding acquisition:* Marjan Enayati, Bruno K. Podesser, Helga Bergmeister

*Investigation:* Marjan Enayati, Christopher Riedmüller, Sabrina Rohringer, Felix Pointner, Lukas Weber, Emir Benca, Marvin Dötzlhofer, Ana Isabel Antunes Goncalves

*Methodology:* Francesco Moscato

*Supervision:* Marjan Enayati

*Writing–original draft:* Marjan Enayati, Christopher Riedmüller, Sabrina Rohringer, Helga Bergmeister

*Writing–review and editing:* Christopher Riedmüller, Sabrina Rohringer, Francesco Moscato, Bruno K. Podesser, Karl H. Schneider, Helga Bergmeister

## Ethics approvals and consent to participate

All the procedures were approved by the Institutional Ethics Committee of the Medical University of Vienna (EK-Nr. regarding the placenta tissue: 1602/2018) and (EK-NR. regarding donated human blood: 2321/2020). Briefly, the donated placentas were obtained from cesarean sections performed at the Department of Obstetrics and Gynecology at the Medical University of Vienna (Austria), after written informed consent of the mothers and approval by the Medical University of Vienna ethics committee (EK:1602/2018). Additionally, the healthy male and female volunteers without anti-coagulant therapy were subjected to venepuncture after verbal informed consent of the blood donor and after approval of the Medical University of Vienna ethics committee (EK: 2321/2020).

## Consent for publication

Not applicable.

## Availability of data

Data will be made available from the corresponding author upon reasonable request.

## References

1. Tsao CW, Aday AW, Almarzooq ZI, et al. Heart disease and stroke statistics—2022 update: a report from the American heart association. *Circulation*. 2022;145(8):e153-e639. doi: 10.1161/CIR.0000000000001052

2. Frangogiannis NG. The extracellular matrix in myocardial injury, repair, and remodeling. *J Clin Invest*. 2017;127(5): 1600-1612. doi: 10.1172/jci87491

3. Nielsen SH, Mouton AJ, DeLeon-Pennell KY, Genovese F, Karsdal M, Lindsey ML. Understanding cardiac extracellular matrix remodeling to develop biomarkers of myocardial infarction outcomes. *Matrix Biol*. 2019;75-76:43-57. doi: 10.1016/j.matbio.2017.12.001

4. Richbourg NR, Peppas NA, Sikavitsas VI. Tuning the biomimetic behavior of scaffolds for regenerative medicine through surface modifications. *J Tissue Eng Regen Med*. 2019;13(8):1275-1293. doi: 10.1002/term.2859

5. Sutthiwanjampa C, Hong S, Kim WJ, Kang SH, Park H. Hydrophilic modification strategies to enhance the surface biocompatibility of poly(dimethylsiloxane)-based biomaterials for medical applications. *Adv Mater Interf*. 2023;10(12):2202333.
doi: 10.1002/admi.202202333

6. Ghaedamini Sl, Karbasi S, Hashemibeni B, Honarvar A, Rabiei A. PCL/Agarose 3D-printed scaffold for tissue engineering applications: fabrication, characterization, and cellular activities. *Res Pharm Sci*. 2023;18(5):566-579.
doi: 10.4103/1735-5362.383711

7. Rashidi N, Najmoddin N, Tavakoli AH, Samanipour R. 3D printed hetero-layered composite scaffold with engineered superficial zone promotes osteogenic differentiation of pre-osteoblast MC3T3-E1 cells. *Surf Interfaces*. 2024;51:104683.
doi: 10.1016/j.surfin.2024.104683

8. Rezaei H, Matin AA, Mohammadnejad M. Cold atmospheric plasma treated 3D printed polylactic acid film; application in thin film solid phase microextraction of anticancer drugs. *Talanta*. 2024;266:125064.
doi: 10.1016/j.talanta.2023.125064

9. Ebrahimi Z, Irani S, Ardeshirylajimi A, Seyedjafari E. Enhanced osteogenic differentiation of stem cells by 3D printed PCL scaffolds coated with collagen and hydroxyapatite. *Sci Rep-UK*. 2022;12(1):12359.
doi: 10.1038/s41598-022-15602-y

10. García AJ, Reyes CD. Bio-adhesive surfaces to promote osteoblast differentiation and bone formation. *J Dent Res*. 2005;84(5):407-413.
doi: 10.1177/154405910508400502

11. Sarker M, Park S, Kumar V, Lee CH. Micro-thin hydrogel coating integrated in 3D printing for spatiotemporal delivery of bioactive small molecules. *Biofabrication*. 2025;17(1): 015019.
doi: 10.1088/1758-5090/ad89fe

12. Pei M, Hwangbo H, Kim G. Hierarchical fibrous collagen/poly(ε-caprolactone) structure fabricated with a 3D-printing process for tissue engineering applications. *Comp B Eng*. 2023;259:110730.
doi: 10.1016/j.compositesb.2023.110730

13. Loyo C, Palza H, Saavedra M, et al. Electrospun polycaprolactone/graphene oxide scaffolds with secondary surface porosity and gelatin-coating. *Mater Today Commun*. 2024;39:109057.
doi: 10.1016/j.mtcomm.2024.109057

14. Zhu J, Li Z, Zou Y, et al. Advanced application of collagen-based biomaterials in tissue repair and restoration. *J Leather Sci Eng*. 2022;4(1):30.
doi: 10.1186/s42825-022-00102-6

15. Lukin I, Erezuma I, Maeso L, et al. Progress in gelatin as biomaterial for tissue engineering. *Pharmaceutics*. 2022;14(6):1177.
doi: 10.3390/pharmaceutics14061177

16. Al-Yafeai Z, Yurdagul A, Peretik JM, Alfaidi M, Murphy PA, Orr AW. Endothelial FN (Fibronectin) deposition by α5β1 integrins drives atherogenic inflammation. *Arterioscler Thromb Vasc Biol*. 2018;38(11):2601-2614.
doi: 10.1161/atvbaha.118.311705

17. Kang BJ, Kim H, Lee SK, et al. Umbilical-cord-blood-derived mesenchymal stem cells seeded onto fibronectin-immobilized polycaprolactone nanofiber improve cardiac function. *Acta Biomater*. 2014;10(7):3007-3017.
doi: 10.1016/j.actbio.2014.03.013

18. Neishabouri A, Soltani Khaboushan A, Daghigh F, Kajbafzadeh AM, Majidi Zolbin M. Decellularization in tissue engineering and regenerative medicine: evaluation, modification, and application methods. *Front Bioeng Biotechnol*. 2022;10:805299.
doi: 10.3389/fbioe.2022.805299

19. Dwivedi R, Kumar S, Pandey R, et al. Polycaprolactone as biomaterial for bone scaffolds: review of literature. *J Oral Biol Craniofac Res*. 2020;10(1):381-388.
doi: 10.1016/j.jobcr.2019.10.003

20. Hu Z, Luo Y, Ni R, et al. Biological importance of human amniotic membrane in tissue engineering and regenerative medicine. *Mater Today Bio*. 2023;22:100790.
doi: 10.1016/j.mtbio.2023.100790

21. Kim JT, Kim KW, Mun SK, Chun YS, Kim JC. Transplantation of autologous perichondrium with amniotic membrane for progressive scleral necrosis. *The Ocular Surface*. 2019;17(3):571-577.
doi: 10.1016/j.jtos.2019.05.004

22. DiDomenico LA, Orgill DP, Galiano RD, et al. Use of an aseptically processed, dehydrated human amnion and chorion membrane improves likelihood and rate of healing in chronic diabetic foot ulcers: a prospective, randomised, multi-centre clinical trial in 80 patients. *Int Wound J*. 2018;15(6):950-957.
doi: 10.1111/iwj.12954

23. Jiang Y, Sun SJ, Zhen Z, et al. Myocardial repair of bioengineered cardiac patches with decellularized placental scaffold and human-induced pluripotent stem cells in a rat model of myocardial infarction. *Stem Cell Res Ther*. 2021;12(1):13.
doi: 10.1186/s13287-020-02066-y

24. Francis MP, Breathwaite E, Bulysheva AA, et al. Human placenta hydrogel reduces scarring in a rat model of cardiac ischemia and enhances cardiomyocyte and stem cell cultures. *Acta Biomater*. 2017;52:92-104.
doi: 10.1016/j.actbio.2016.12.027

25. Duan Y, Huang W, Zhan B, et al. Bioink derived from human placenta supporting angiogenesis. *Biomed Mater*. 2022;17(5).
doi: 10.1088/1748-605X/ac7b5b

26. Schneider KH, Goldberg BJ, Hasturk O, et al. Silk fibroin, gelatin, and human placenta extracellular matrix-based

composite hydrogels for 3D bioprinting and soft tissue engineering. *Biomater Res.* 2023;27(1):117. doi: 10.1186/s40824-023-00431-5

27. Khosrowpour Z, Bashiri Z, Jafari D, et al. Translation prospects of a novel ECM-silk fibroin/alginate 3D-printed scaffold for treatment of full-thickness skin wounds: an *in vitro* and *in vivo* study. *Polym Adv Technol*. 2024;35(11):e6637. doi: 10.1002/pat.6637

28. Lakkireddy C, Vishwakarma SK, Raju N, et al. Fabrication of decellularized amnion and chorion scaffolds to develop bioengineered cell-laden constructs. *Cell Mol Bioeng*. 2022;15(1):137-150. doi: 10.1007/s12195-021-00707-7

29. Patel HN, Vohra YK, Singh R, Thomas V. HuBiogel incorporated fibro-porous hybrid nanomatrix graft for vascular tissue interfaces. *Mater Today Chem*. 2020;17: 100323. doi: 10.1016/j.mtchem.2020.100323.

30. Lei J, Priddy LB, Lim JJ, Koob TJ. Dehydrated human amnion/chorion membrane (dHACM) allografts as a therapy for orthopedic tissue repair. *Tech Orthop*. 2017;32(3):149-157. doi: 10.1097/bto.0000000000000229

31. Go YY, Chae SW, Song JJ. Osteogenic effects of exosomes derived from human chorion membrane extracts. *Biomater Res*. 2021;25(1):16. doi: 10.1186/s40824-021-00218-6

32. Flores-Espinosa P, Méndez I, Irles C, et al. Immunomodulatory role of decidual prolactin on the human fetal membranes and placenta. *Frontiers in Immunology*. 2023;14:1212736. doi: 10.3389/fimmu.2023.1212736

33. McQuilling JP, Vines JB, Kimmerling KA, Mowry KC. Proteomic comparison of amnion and chorion and evaluation of the effects of processing on placental membranes. *Wounds*. 2017;29(6):E36-E40.

34. Schneider KH, Enayati M, Grasl C, et al. Acellular vascular matrix grafts from human placenta chorion: impact of ECM preservation on graft characteristics, protein composition and *in vivo* performance. *Biomaterials*. 2018;177:14-26. doi: 10.1016/j.biomaterials.2018.05.045

35. Rohringer S, Schneider KH, Eder G, et al. Chorion-derived extracellular matrix hydrogel and fibronectin surface coatings show similar beneficial effects on endothelialization of expanded polytetrafluorethylene vascular grafts. *Mater Today Bio*. 2022;14:100262. doi: 10.1016/j.mtbio.2022.100262

36. Kaniuk E, Lechowska-Liszka A, Gajek M, et al. Correlation between porosity and physicochemical and biological properties of electrospinning PLA/PVA membranes for skin regeneration. *Biomater Adv*. 2023;152:213506. doi: 10.1016/j.bioadv.2023.213506

37. Grasl C, Bergmeister H, Stoiber M, Schima H, Weigel G. Electrospun polyurethane vascular grafts: *in vitro* mechanical behavior and endothelial adhesion molecule expression. *J Biomed Mater Res A*. 2010;93a(2):716-723. doi: 10.1002/jbm.a.32584

38. Janssen D, De Palma R, Verlaak S, Heremans P, Dehaen W. Static solvent contact angle measurements, surface free energy and wettability determination of various self-assembled monolayers on silicon dioxide. *Thin Solid Films*. 2006;515(4):1433-1438. doi: 10.1016/j.tsf.2006.04.006

39. Thaler B, Baik N, Hohensinner PJ, et al. Differential expression of Plg-R(KT) and its effects on migration of proinflammatory monocyte and macrophage subsets. *Blood*. 2019;134(6):561-567. doi: 10.1182/blood.2018850420

40. Silvestri A, Boffito M, Sartori S, Ciardelli G. Biomimetic materials and scaffolds for myocardial tissue regeneration. *Macromol Biosci*. 2013;13(8):984-1019. doi: 10.1002/mabi.201200483

41. Liu T, Hao Y, Zhang Z, et al. Advanced cardiac patches for the treatment of myocardial infarction. *Circulation*. 2024;149(25):2002-2020. doi: 10.1161/CIRCULATIONAHA.123.067097

42. Kakabadze Z, Kakabadze A, Chakhunashvili D, et al. Decellularized human placenta supports hepatic tissue and allows rescue in acute liver failure. *Hepatology*. 2018;67(5):1956-1969. doi: 10.1002/hep.29713

43. Kim BS, Kim H, Gao G, Jang J, Cho DW. Decellularized extracellular matrix: a step towards the next generation source for bioink manufacturing. *Biofabrication*. 2017;9(3):034104. doi: 10.1088/1758-5090/aa7e98

44. Prince E, Kumacheva E. Design and applications of man-made biomimetic fibrillar hydrogels. *Nat Rev Mater.* 2019;4(2):99-115. doi: 10.1038/s41578-018-0077-9

45. Schneider KH, Aigner P, Holnthoner W, et al. Decellularized human placenta chorion matrix as a favorable source of small-diameter vascular grafts. *Acta Biomater*. 2016;29:125-134. doi: 10.1016/j.actbio.2015.09.038

46. Ferreira SA, Motwani MS, Faull PA, et al. Bi-directional cell-pericellular matrix interactions direct stem cell fate. *Nat Commun.* 2018;(1):4049. doi: 10.1038/s41467-018-06183-4

47. Huebsch N, Arany PR, Mao AS, et al. Harnessing traction-mediated manipulation of the cell/matrix interface to control stem-cell fate. *Nat Mater*. 2010;9(6):518-526. doi: 10.1038/nmat2732

48. Simmons CA, Alsberg E, Hsiong S, Kim WJ, Mooney DJ. Dual growth factor delivery and controlled scaffold degradation enhance *in vivo* bone formation by transplanted bone marrow stromal cells. *Bone*. 2004;35(2):562-569. doi: 10.1016/j.bone.2004.02.027

49. Tang J, Vandergriff A, Wang Z, et al. A regenerative cardiac patch formed by spray painting of biomaterials onto the heart. *Tissue Eng Part C Methods*. 2017;23(3):146-155. doi: 10.1089/ten.TEC.2016.0492

50. Rebollar E, Frischauf I, Olbrich M, et al. Proliferation of aligned mammalian cells on laser-nanostructured polystyrene. *Biomaterials*. 2008;29(12):1796-1806. doi: 10.1016/j.biomaterials.2007.12.039

51. Paragkumar T, Edith ND, Six JL. Surface characteristics of PLA and PLGA films. *Appl Surf Sci*. 2006;253(5):2758-2764. doi: 10.1016/j.apsusc.2006.05.047

52. Kapnisi M, Mansfield C, Marijon C, et al. Auxetic cardiac patches with tunable mechanical and conductive properties toward treating myocardial infarction. *Adv Funct Mater*. 2018;28(21):1800618. doi: 10.1002/adfm.201800618

53. Wall ST, Walker JC, Healy KE, Ratcliffe MB, Guccione JM. Theoretical impact of the injection of material into the myocardium: a finite element model simulation. *Circulation*. 2006;114(24):2627-2635. doi: 10.1161/circulationaha.106.657270

54. Saraswathibhatla A, Indana D, Chaudhuri O. Cell–extracellular matrix mechanotransduction in 3D. *Nat Rev Mol Cell Biol*. 2023;24(7):495-516. doi: 10.1038/s41580-023-00583-1

55. Yang B, Wei K, Loebel C, et al. Enhanced mechanosensing of cells in synthetic 3D matrix with controlled biophysical dynamics. *Nat Commun*. 2021;12(1):3514. doi: 10.1038/s41467-021-23120-0

56. Gautieri A, Vesentini S, Redaelli A, Buehler MJ. Hierarchical structure and nanomechanics of collagen microfibrils from the atomistic scale up. *Nano Lett*. 2011;11(2):757-766. doi: 10.1021/nl103943u

57. Vader D, Kabla A, Weitz D, Mahadevan L. Strain-induced alignment in collagen gels. *PLoS One*. 2009;4(6):e5902. doi: 10.1371/journal.pone.0005902

58. Kolliopoulos V, Dewey MJ, Polanek M, Xu H, Harley BAC. Amnion and chorion matrix maintain hMSC osteogenic response and enhance immunomodulatory and angiogenic potential in a mineralized collagen scaffold. *Front Bioeng Biotechnol*. 2022;10:1034701. doi: 10.3389/fbioe.2022.1034701

59. Soundararajan M, Kannan S. Fibroblasts and mesenchymal stem cells: two sides of the same coin?. *J Cell Physiol*. 2018;233(12):9099-9109. doi: 10.1002/jcp.26860

60. Costa-Almeida R, Gomez-Lazaro M, Ramalho C, Granja PL, Soares R, Guerreiro SG. Fibroblast-endothelial partners for vascularization strategies in tissue engineering. *Tissue Eng Part A*. 2015;21(5-6):1055-1065. doi: 10.1089/ten.TEA.2014.0443

61. Loureiro J, Miguel SP, Galván-Chacón V, et al. Three-dimensionally printed hydrogel cardiac patch for infarct regeneration based on natural polysaccharides. *Polymers*. 2023;15(13):2824. doi: 10.3390/polym15132824

62. Virag JI, Murry CE. Myofibroblast and endothelial cell proliferation during murine myocardial infarct repair. *Am J Pathol*. 2003;163(6):2433-2440. doi: 10.1016/S0002-9440(10)63598-5

63. Caneparo C, Baratange C, Chabaud S, Bolduc S. Conditioned medium produced by fibroblasts cultured in low oxygen pressure allows the formation of highly structured capillary-like networks in fibrin gels. *Sci Rep-UK*. 2020; 10(1):9291. doi: 10.1038/s41598-020-66145-z

64. Kunz-Schughart LA, Schroeder JA, Wondrak M, et al. Potential of fibroblasts to regulate the formation of three-dimensional vessel-like structures from endothelial cells *in vitro*. *Am J Physiol Cell Physiol*. 2006;290(5):C1385-C1398. doi: 10.1152/ajpcell.00248.2005

65. Amin K, Dannenfelser RM. *In vitro* hemolysis: guidance for the pharmaceutical scientist. *J Pharm Sci*. 2006;95(6): 1173-1176. doi: 10.1002/jps.20627

66. Huang H, Huang W. Regulation of endothelial progenitor cell functions in ischemic heart disease: new therapeutic targets for cardiac remodeling and repair. *Front Cardiovasc Med*. 2022;9:896782. doi: 10.3389/fcvm.2022.896782

67. Du F, Zhou J, Gong R, et al. Endothelial progenitor cells in atherosclerosis. *Front Biosci (Landmark Ed)*. 2012;17(6): 2327-2349. doi: 10.2741/4055

68. Yoder MC. Human endothelial progenitor cells. *Cold Spring Harb Perspect Med*. 2012;2(7):a006692. doi: 10.1101/cshperspect.a006692

69. Clauder F, Czerniak AS, Friebe S, Mayr SG, Scheinert D, Beck-Sickinger AG. Endothelialization of titanium surfaces by bioinspired cell adhesion peptide coatings. *Bioconjug Chem*. 2019;30(10):2664-2674. doi: 10.1021/acs.bioconjchem.9b00573

70. Ardila DC, Liou JJ, Maestas D, et al. Surface modification of electrospun scaffolds for endothelialization of tissue-engineered vascular grafts using human cord blood-derived endothelial cells. *J Clin Med*. 2019;8(2):185. doi: 10.3390/jcm8020185

71. Sgarioto M, Vigneron P, Patterson J, Malherbe F, Nagel MD, Egles C. Collagen type I together with fibronectin provide a better support for endothelialization. *C R Biol*. 2012;335(8):520-528. doi: 10.1016/j.crvi.2012.07.003

72. Kaur R, Singh V, Kumari P, Singh R, Chopra H, Emran TB. Novel insights on the role of VCAM-1 and ICAM-1: potential biomarkers for cardiovascular diseases. *Ann Med Surg (Lond)*. 2022;84:104802. doi: 10.1016/j.amsu.2022.104802

73. Lertkiatmongkol P, Liao D, Mei H, Hu Y, Newman PJ. Endothelial functions of platelet/endothelial cell adhesion molecule-1 (CD31). *Curr Opin Hematol*. 2016;23(3):253-259. doi: 10.1097/moh.0000000000000239

74. Bačáková L, Mareš V, Lisá V, Švorčík V. Molecular mechanisms of improved adhesion and growth of an endothelial cell line cultured on polystyrene implanted with fluorine ions. *Biomaterials*. 2000;21(11):1173-1179. doi: 10.1016/S0142-9612(00)00009-0

75. Post A, Wang E, Cosgriff-Hernandez E. A review of integrin-mediated endothelial cell phenotype in the design of cardiovascular devices. *Ann Biomed Eng*. 2019;47(2):366-380. doi: 10.1007/s10439-018-02171-3

76. Kimes BW, Brandt BL. Properties of a clonal muscle cell line from rat heart. *Exp Cell Res*. 1976;98(2):367-381. doi: 10.1016/0014-4827(76)90447-x

77. Watkins SJ, Borthwick GM, Arthur HM. The H9C2 cell line and primary neonatal cardiomyocyte cells show similar hypertrophic responses *in vitro*. *In Vitro Cell Dev Biol Anim*. 2011;47(2):125-131. doi: 10.1007/s11626-010-9368-1

78. Branco AF, Pereira SP, Gonzalez S, Gusev O, Rizvanov AA, Oliveira PJ. Gene expression profiling of H9c2 myoblast differentiation towards a cardiac-like phenotype. *PLoS One*. 2015;10(6):e0129303. doi: 10.1371/journal.pone.0129303.

79. Branco AF, Sampaio SF, Wieckowski MR, Sardão VA, Oliveira PJ. Mitochondrial disruption occurs downstream from β-adrenergic overactivation by isoproterenol in differentiated, but not undifferentiated H9c2 cardiomyoblasts: differential activation of stress and survival pathways. *Int J Biochem Cell Biol*. 2013;45(11):2379-2391. doi: 10.1016/j.biocel.2013.08.006

80. Arıcı Ş, Kamali AR, Ege D. CMC/Gel/GO 3D-printed cardiac patches: GO and CMC improve flexibility and promote H9C2 cell proliferation, while EDC/NHS enhances stability. *Biofabrication*. 2025;17(1):015025. doi: 10.1088/1758-5090/ad8e87

81. Bertani FR, Mozetic P, Fioramonti M, et al. Classification of M1/M2-polarized human macrophages by label-free hyperspectral reflectance confocal microscopy and multivariate analysis. *Sci Rep-UK*. 2017;7(1):8965. doi: 10.1038/s41598-017-08121-8

82. Rey-Giraud F, Hafner M, Ries CH. *In vitro* generation of monocyte-derived macrophages under serum-free conditions improves their tumor promoting functions. *PLoS One*. 2012;7(8):e42656. doi: 10.1371/journal.pone.0042656

83. Yue B. Biology of the extracellular matrix: an overview. *J Glaucoma*. 2014;23(8 Suppl 1):S20-S23. doi: 10.1097/ijg.0000000000000108

84. Mehanna RA, Essawy MM, Barkat MA, et al. Cardiac stem cells: current knowledge and future prospects. *World J Stem Cells*. 2022;14(1):1-40. doi: 10.4252/wjsc.v14.i1.1